Effects of continental-scale snow albedo anomalies on the wintertime Arctic oscillation

R. J. Allen[1] and C. S. Zender[1]

Received 12 May 2010; revised 9 September 2010; accepted 13 September 2010; published 3 December 2010.

[1] The NCAR CAM3 GCM with prescribed, satellite-based snow albedo (SA) is used to investigate the remote effects of snow cover on Northern Hemisphere (NH) winter climate. A pair of 100 ensemble member experiments are integrated through the autumn-winter season, with prescribed high and low SA over Eurasia (EA). Similar to other non-CAM GCM studies using prescribed snow mass, anomalous EA snow albedo produces a wave activity pulse that propagates into the stratosphere, culminating in a negative phase Arctic Oscillation– (AO-) like surface response. This occurs for idealized but representative SA anomalies, as well as for more realistic SA anomalies. Similar experiments over North America (NA) and the entire NH are also performed. Unlike prior studies, anomalous NA snow yields a significant AO signal. Here, the local NA surface cooling elicits a transient eddy response, which propagates downstream to Eurasia, resulting in significant but short-lived cooling and upward propagating wave activity over Siberia. A negative AO-like response develops, primarily confined to the stratosphere/upper troposphere, which eventually gives way to a tropospheric AO-like response of the opposite phase, due to equatorward wave refraction and wave divergence. Reanalysis data support this NA snow-positive AO response. Snow forcing experiments for the whole NH, however, yield a weakened AO signal. This is due to a muted wavenumber-1 and -2 response caused by destructive interference between the background stationary wave and the corresponding Rossby wave response, which results in negligible wave activity reaching the stratosphere.

Citation: Allen, R. J., and C. S. Zender (2010), Effects of continental-scale snow albedo anomalies on the wintertime Arctic oscillation, *J. Geophys. Res.*, *115*, D23105, doi:10.1029/2010JD014490.

1. Introduction

[2] The dominant mode of extratropical Northern Hemisphere (NH) wintertime atmospheric circulation variability is referred to as the Arctic Oscillation (AO) [*Thompson and Wallace*, 1998] or the Northern Annular Mode (NAM) [*Thompson and Wallace*, 2001]. This pattern of variability is associated with an oscillation of atmospheric mass between high latitudes and midlatitudes, which occurs over a range of time scales, from intraseasonal to interdecadal. The AO also contains expressions in surface air temperature, precipitation, total column ozone, and tropopause height [*Thompson and Wallace*, 2000]. Although it exists year round in the troposphere, the AO is strongest during winter, when the atmosphere is conducive to strong planetary wave-mean flow interaction. During this active season, the AO extends upward through the stratosphere and is associated with fluctuations in the polar vortex.

[3] The regional manifestation of the AO/NAM in the North Atlantic, the North Atlantic Oscillation (NAO) [*Wallace and Gutzler*, 1981; *Hurrell and van Loon*, 1997], is similar and is associated with opposite phased temperature and pressure oscillations between the Icelandic low and the Azores high. The NAO affects the strength and direction of westerly winds, storm tracks and precipitation across the North Atlantic, as well as the frequency of occurrence of high-latitude blocking and cold air outbreaks throughout the hemisphere [*Thompson and Wallace*, 2001]. Both the NAO and AO exhibited positive trends for much of the 1970s and 1980s, with historic highs in the early 1990s, which likely contribute to global warming [*Thompson et al.*, 2000].

[4] Both the NAO and AO appear to be fundamental, internal modes of the atmosphere, because they exist in uncoupled models forced by climatological SSTs [e.g., *Robertson*, 2001; *Gong et al.*, 2002]. However, they may be modulated by external forcings [*Shindell et al.*, 1999; *Feldstein*, 2002; *Gong et al.*, 2002]. Although several such external forcings have been identified, no dominant mechanism has been clearly established. These forcings include SSTs, over the North Atlantic [*Rodwell et al.*, 1999; *Robertson et al.*, 2000] and the Indo-Pacific warm pool [*Hoerling et al.*, 2001; *Hurrell et al.*, 2004; *Selten et al.*,

[1]Department of Earth System Science, University of California, Irvine, California, USA.

Copyright 2010 by the American Geophysical Union.
0148-0227/10/2010JD014490

2004], as well as greenhouse gases (GHGs) and ozone [*Shindell et al.*, 1999; *Fyfe et al.*, 1999; *Osborn*, 2004; *Miller et al.*, 2006], volcanic aerosols [*Stenchikov et al.*, 2002, 2006] and Eurasian snow cover [e.g., *Cohen and Entekhabi*, 1999].

[5] The impact of snow on local climate is well documented: winter months with anomalously high snow cover are associated with below-normal temperatures, due to changes in the surface energy balance [e.g., *Wagner*, 1973; *Leathers and Robinson*, 1993; *Leathers et al.*, 1995]. The main mechanism responsible is reduced shortwave radiation due to increased albedo, although other thermodynamic mechanisms also exist, including increased thermal emissivity, decreased thermal conductivity and increased latent heat due to snow melt [*McFadden and Ragotzkie*, 1967; *Dewey*, 1977; *Walland and Simmonds*, 1996; *Gong et al.*, 2004]. Snow cover can also affect remote climate. For example, significant observational evidence exists relating Eurasian autumn snow cover to the subsequent winter's AO, influencing it's phase, strength and interannual variability [e.g., *Cohen and Entekhabi*, 1999; *Saito and Cohen*, 2003; *Cohen and Barlow*, 2005]. Moreover, *Cohen and Barlow* [2005] show that October Eurasian snow cover anomalies, and not the other aforementioned mechanisms, has likely forced the AO. Over the last 16 years, EA snow cover is best matched with the AO in terms of both pattern and trend, with similar decadal swings in both, and no mismatch where trends are present in the AO, but not the mechanism.

[6] Observations also support a snow-AO mechanism, whereby anomalously high EA snow cover results in an increase in upward stationary Rossby waves, which deposit their easterly momentum in the stratosphere, slowing the polar vortex and increasing polar cap geopotential heights, resulting in a negative stratospheric AO. This anomaly then propagates downward through the troposphere [*Haynes et al.*, 1991; *Baldwin and Dunkerton*, 1999, 2001], resulting in a negative AO-like response at the surface [*Saito et al.*, 2001; *Cohen et al.*, 2007; *Hardiman et al.*, 2008].

[7] GCM studies with freely varying snow are unable to reproduce the observed snow-AO relationship (both AGCMs and coupled models). This includes the correlation between October EA snow anomalies and the winter AO [*Cohen et al.*, 2005], as well as the correlation between October EA snow anomalies and upward propagating wave activity [*Hardiman et al.*, 2008]. Model deficiencies in snow cover, in particular interannual variations, are likely responsible, as most GCMs underestimate EA snow cover interannual variability [*Frei et al.*, 2003; *Roesch*, 2006; *Hardiman et al.*, 2008].

[8] When Eurasian snow is prescribed in GCMs, however, a snow-AO relationship similar to observations exists [e.g., *Gong et al.*, 2002, 2003a; *Fletcher et al.*, 2007, 2009]. Prescribed snow experiments are also consistent with the proposed snow-AO mechanism, with positive EA snow anomalies leading to enhanced vertical wave flux into the stratosphere, that eventually yields a negative AO-like pattern at the surface [*Gong et al.*, 2003a; *Fletcher et al.*, 2007, 2009].These results, however, may depend on model details, such as stratospheric representation and orographic gravity wave drag parameterization [*Sigmond et al.*, 2008; *Shaw et al.*, 2009; *Fletcher et al.*, 2009].

[9] There have been relatively few studies investigating the remote effects of North American (NA) snow on winter climate, with observational and modeling studies yielding conflicting results. Based on observations, *Dickson and Namias* [1976] showed NA snow cover, through enhanced baroclinicity, shifted the North Atlantic storm tracks southward, implying the negative NAO phase. In a more recent analysis, *Saito and Cohen* [2003] showed the only significant relationship between NA snow and remote climate was a negative correlation between summer NA snow and the winter AO; no significant NAO correlations existed. GCM studies, however, generally suggest NA snow forces a positive AO/NAO (opposite to EA snow). *Gong et al.* [2003b] found fall NA snow forcing yielded a weak increase in vertically propagating wave activity, but confined to the troposphere. However, enhanced equatorward wave activity in the troposphere, associated with a poleward momentum flux, resulted in a weak, positive AO-like surface response. This is consistent with *Klingaman et al.* [2008] who showed snow cover over the northern Great Plains of the United States forced a positive NAO, but not until late winter (January–February). Although *Sobolowski et al.* [2007] did not find a NAO/AO-like response to NA snow forcing, they did find a significant remote response, including increased wintertime surface temperatures and reduced sea-level pressures over Europe, due to a strengthening and eastward shift of the low-level stationary wave pattern. Similarly, [*Sobolowski et al.*, 2010] found significant Eurasian surface warming during spring, involving downstream propagation of a transient eddy response from the NA snow forcing region to Eurasia. Such a response, however only occurred for experiments integrated over the entire year; similar experiments integrated over the fall season yielded a muted response.

[10] In this paper, we present snow-AO experiments with the National Center for Atmospheric Research (NCAR) Community Atmosphere Model (CAM3), focusing on the remote effects of EA, NA, and NH snow cover. Similar to prior GCM results, we show that EA snow cover is able to affect climate remotely and modulate the dominant mode of NH wintertime atmospheric circulation variability. We also show that this response is primarily caused by snow-induced increases in surface albedo. This occurs for both idealized snow albedo (SA) anomalies, as well as for more realistic SA anomalies. We also show that NA snow cover can have a significant remote effect on NH winter climate, which is also supported by observations. Although the evolution of EA and NA responses, and the net effect on the AO are different, similar mechanisms, involving large-scale Rossby waves and tropospheric-stratospheric coupling, are involved with both. However, higher-frequency, synoptic-scale transient eddies associated with the increase in temperature gradient and baroclinicity over NA are also involved with the NA snow response. Finally, we show that snow forcing over the entire NH yields a muted AO signal, due to minimal propagation of the Rossby wave response from the troposphere to the stratosphere. This is related to destructive interference between the stationary background wave and the corresponding response. This paper is organized as follows. Section 2 describes our snow prescription method and experimental design. Results are presented in section 3, including the effects of Eurasian, North American,

and Northern Hemisphere snow albedo on remote atmospheric circulation, as well as a discussion of the physical mechanisms involved. A discussion, with a brief comparison of the EA and NA results to observations, is presented in section 4. Conclusions follow in section 5.

2. Methods

2.1. CAM Description

[11] The Community Atmosphere Model (CAM) version 3 [*Collins et al.*, 2004], is the fifth generation of the National Center for Atmosphere Research (NCAR) atmospheric General Circulation Model (GCM) and is the atmospheric component of the Community Climate System Model (CCSM). CAM uses a Eulerian spectral transform dynamical core, where variables are represented in terms of coefficients of a truncated series of spherical harmonic functions. The model time step is 20 min, and time integration is performed with a semi-implicit leapfrog scheme. The vertical coordinate is a hybrid coordinate, with 26 vertical levels. The model has a relatively poorly resolved stratosphere, with ~9 levels above 100 hPa and a top level at 2.9 hPa. The total parameterization package consists of four basic components: moist precipitation processes/convection, clouds and radiation, surface processes, and turbulent mixing. In addition, orographic gravity wave drag, which controls the strength of the zonal wind in the midlatitude to high-latitude lower stratosphere, is similar to the *McFarlane* [1987] parameterization, which is based on the surface stress generated. Studies have shown that boundary conditions on parameterized gravity wave fluxes can affect coupled stratosphere-troposphere responses to climate perturbations (such as snow cover) at high latitudes [*Sigmond et al.*, 2008; *Shaw et al.*, 2009]; investigating such effects is beyond the scope of this study. The land surface model is the Community Land Model (CLM) version 3 [*Oleson et al.*, 2004], which combines realistic radiative, ecological and hydrologic processes.

2.2. Prescribed Snow Method

[12] Past approaches at specifying snow have prescribed snow mass [*Gong et al.*, 2002, 2003a; *Fletcher et al.*, 2007, 2009]. At each model time step, the model-derived snow mass is replaced with a prescribed value. Snow is allowed to fall and accumulate as normal and melting of the existing snow can occur, releasing latent heat to the atmosphere and soil moisture to the land. By artificially creating or destroying snow mass, water and energy are not conserved. For example, *Gong et al.* [2004] suggest that a large and abrupt introduction of prescribed snow during the warmer autumn months likely leads to more snow melt, leading to an exaggerated latent heat flux. *Fletcher et al.* [2009] however, found a similar, but weaker response, if the snow perturbation is allowed to melt, rather than being held fixed, after it is first prescribed.

[13] We prescribe snow using an alternate procedure, by incorporating its effects on surface albedo. We therefore implicitly neglect other snow-related mechanisms that may contribute to changes in the surface energy balance, such as decreased thermal conductivity and increased thermal emissivity. However, because the imposed snow albedo results in significant surface cooling that extends through the low troposphere/midtroposphere, the model's actual snow cover and snow depth are increased over the forcing region. Thus, our prescribed snow method indirectly accounts for nonalbedo mechanisms. Furthermore, because the model's actual snow field is able to freely evolve, this method eliminates the lack of water conservation associated with artificially altering snow mass. Energy conservation, however, may still be an issue.

[14] Monthly snow cover fraction data is obtained from the NOAA satellite data set, based primarily on visible band imagery (see http://climate.rutgers.edu/snowcover/index.php). This is interpolated to the CAM grid and fed into the land model to estimate ground albedo at each time step (see Appendix A). If a land grid cell possess a nonzero, satellite-based snow cover fraction, then a snow albedo is estimated, in accord with equation (A1), neglecting the effects of snow aging. Sensitivity tests showed that soil moisture and freezing lakes/wetlands had relatively small impacts on the overall surface albedo, so these are left unaltered. However, the effects of snow masking vegetation proved to be important, especially during the earlier fall months when trees still possess leaves. We therefore account for this effect on ground albedo by adjusting the exposed lead/stem area (equation (A2)). The final ground albedo is estimated according to equations (A3) and (A4), as a weighted average of soil and snow albedos, using the satellite-based snow cover fraction.

2.3. Experimental Design

[15] CAM is run at T42 resolution (~2.8° × 2.8°) with prescribed, climatological SSTs and sea ice. To obtain robust statistics (because of the large variability in the response) we use a 100-member ensemble of realizations started from independent initial conditions. Each ensemble member is started from a 100 year control integration of CAM forced with climatological SSTs and sea ice with fixed atmospheric composition. Every 1 October of this 100 year control run, we branch two additional runs, which are integrated through 31 December. The first set of branch runs feature prescribed climatologically high Eurasian (30°N–90°N; 0°–180°E) snow cover, based on the average January EA snow cover from 5 years (1972, 1976, 1977, 1998, 2002), which correspond to the largest EA October snow cover areas. Note that we do not use the five largest EA January snow areas; this makes little difference, however, since a January snow in autumn represents an anomalously high snow. Outside the Eurasian region, snow cover is prescribed using climatologically low snow cover, based on the same 5 years, but using the corresponding September snow field. The second set of branch simulations are similar, except September snow cover is prescribed at each NH land surface grid point. The response to the snow perturbation is defined as the difference between these high- and low-snow branch runs. Once specified, the snow perturbation is held constant throughout each branch run and the forcing comes from the Eurasian region alone. This experiment is referred to as the idealized EA (IEA) experiment.

[16] Figure 1 shows the NOAA satellite-based EA snow cover forcing for these 5 years (January minus September snow fraction). September features relatively little snow cover (2.5%), whereas most of the region is snow covered by January (42.3%), yielding a difference of 39.8%. This

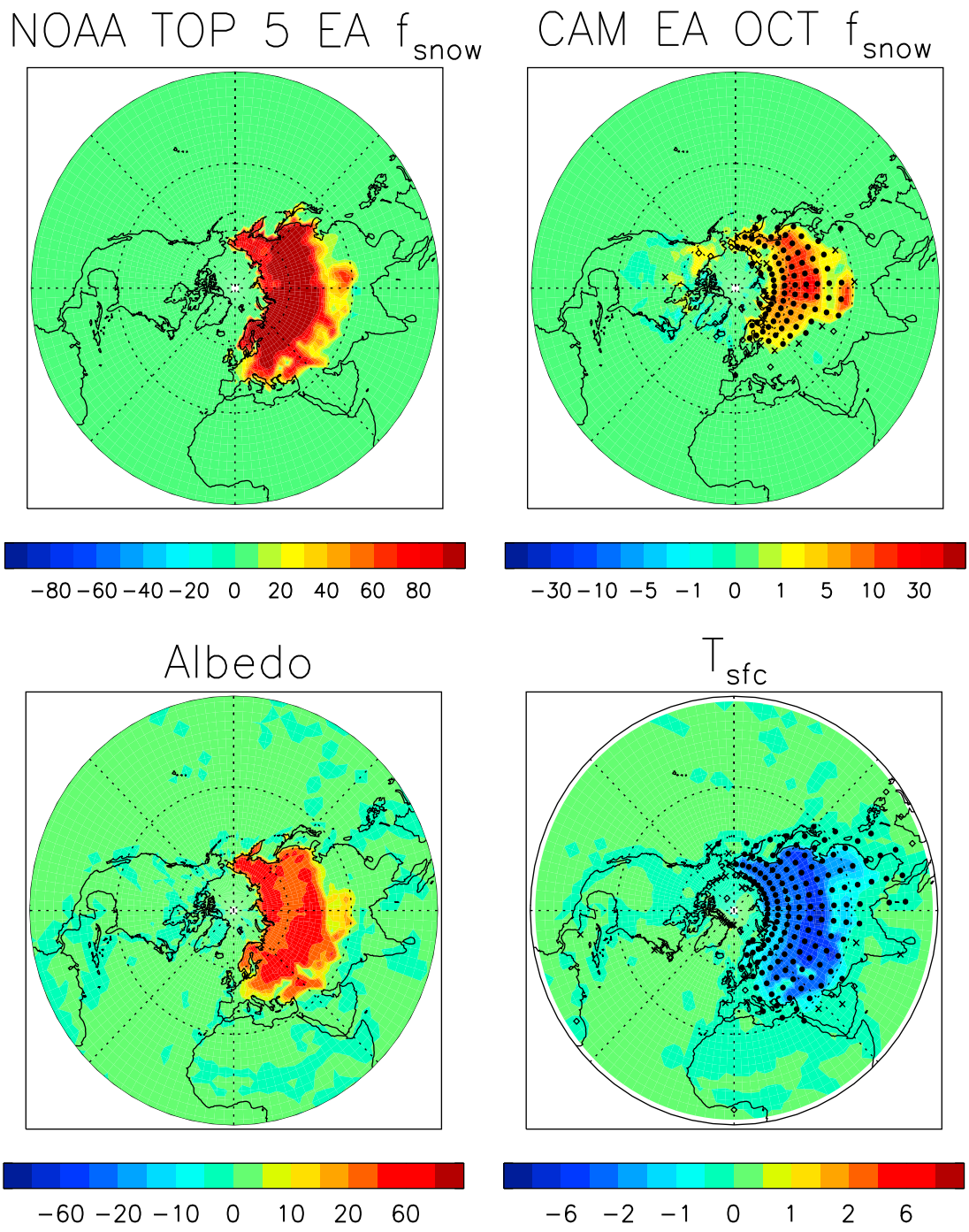

Figure 1. (top) January minus September NOAA EA (30°N–90°N; 0°–180°E) snow cover fraction based on (left) the five largest Octobers and (right) the corresponding October (OCT) f_{snow} CAM ensemble mean response. NOAA EA Δf_{snow} = 39.8%; CAM EA OCT Δf_{snow} = 2.7%. (bottom) October ensemble mean EA (left) snow albedo forcing and (right) surface temperature response. Eurasian OCT mean $\Delta\alpha$ = 22%; ΔT_{sfc} = −1.2 K. Symbols represent significance at the 90% (diamond), 95% (cross), and 99% (dot) confidence level and are plotted every three longitudes and two latitudes.

yields a corresponding albedo forcing (as estimated by CAM) of 22%, which results in a decrease in the net surface solar radiation of −17.5 W m^{-2}, which cools the EA surface by 1.2 K. As mentioned above, this cooling results in the model producing more snow over the forcing region. For October, there is a 2.7% increase in EA snow cover and a 0.6 cm increase in snow depth (not shown); these quantities increase to ~4% and 2 cm, respectively, in November and December. Although the modeled f_{snow} response is much smaller than observed (nor would we expect it to be of the same magnitude, since this is an idealized situation), our

Table 1. Ensemble Mean Pressure-Weighted Spatial Correlations Between WAF_Z and $WAF_{Z,CNT}$ at 60°N (r_{WAF}), Averaged Over Each Experiment's Growth Phase, for All-Waves and Wavenumber-1 Through Wavenumber-4[a]

Experiment	Growth Phase Days	All-Waves	Wavenumber-1	Wavenumber-2	Wavenumber-3	Wavenumber-4
IEA	30–75	0.50	0.80	0.29	0.58	−0.10
$IEA_{1–50}$	30–75	0.25	0.73	−0.23	−0.03	0.02
$IEA_{51–100}$	30–75	0.34	0.68	0.39	0.25	−0.46
REA	40–89	0.32	0.45	0.71	0.29	−0.36
$REA_{1–50}$	40–89	0.41	0.52	0.70	0.38	0.24
$REA_{51–100}$	40–89	0.04	0.20	0.39	0.02	−0.66
NA	60–89	0.07	0.22	−0.25	0.56	−0.18
NH	30–75	−0.09	−0.24	−0.84	0.62	0.48

[a]Also included are two 50-member IEA and REA subsets based on ensemble members 1–50 and 51–100.

prescribed snow procedure weakly accounts for nonalbedo mechanisms.

2.4. Stationary Wave Diagnostic

[17] Thermal forcings have been shown to amplify orographically forced stationary waves [*Ringler and Cook*, 1999] and both observational [*Saito et al.*, 2001; *Cohen et al.*, 2007] and modeling [*Gong et al.*, 2003a; *Fletcher et al.*, 2009] studies have associated upward propagating Rossby waves with anomalously high Siberian snow. In this paper, we use the wave activity flux (WAF) to quantify the upward and poleward propagation of planetary waves. The vertical (WAF_Z) and meridional (WAF_Y) components are written as [*Plumb*, 1985]

$$\mathrm{WAF_Z} = 2p\Omega\cos(\phi)\sin(\phi)S^{-1}\left[v'T' - \frac{1}{2\Omega R_e \sin(2\phi)}\frac{\partial}{\partial\lambda}(T'\Phi')\right] \quad (1)$$

$$\mathrm{WAF_Y} = -u'v' + \frac{1}{2\Omega R_e \sin(2\phi)}\frac{\partial(u'\Phi')}{\partial\lambda}, \quad (2)$$

where variables represent their standard meteorological values, R_e is mean radius of the earth, λ is longitude, ϕ is latitude, Ω is the angular velocity of rotation, S is static stability and primes denote deviations from the zonal mean. WAF_Z is useful for localizing in longitude and latitude the source of vertically propagating stationary Rossby waves and is proportional to the vertical component of the often used quasigeostrophic Eliassen-Palm (EP) flux [*Edmon et al.*, 1980].

3. Results

[18] Similar to *Limpasuvan et al.* [2004] and *Fletcher et al.* [2009], the transient response to anomalous snow cover divides into three distinct phases: onset, growth, and mature. We focus on the growth phase, defined here as the time period from the initial to the peak stratospheric response, as listed in Table 1 for each experiment. The onset and mature phases, therefore, are defined as the time period before and after the growth phase, respectively.

3.1. Eurasia

3.1.1. Idealized Experiments

[19] Figure 2 shows a vertical cross section of the ensemble-mean transient response in polar cap (≥60°N) geopotential height (Z_{PC}), which we use as a representative measure of the AO. During the onset phase, the initial response to idealized EA (IEA) snow forcing is a tropospheric low at high latitudes that extends throughout the atmosphere. As shown by *Smith et al.* [2010], this response is related to destructive interference between the stationary background wave in the control (i.e., low snow) experiment and the corresponding Rossby wave response (to be discussed below). After ~30 days, during the growth phase, Z_{PC} becomes positive in the stratosphere, which is associated with in increase in upward wave activity flux (WAF_Z), first in the troposphere near day 20 and then in the stratosphere 10 days later. The WAF_Z response is centered over the forcing region (not shown), amplifying the naturally occurring, orographically forced upward wave activity over Siberia [*Plumb*, 1985].

[20] Convergence of EP flux, as represented by the northward transport of quasigeostrophic potential vorticity ($\overline{v'q'}$) [*Rind et al.*, 2005a], also occurs above 100 hPa and centered near 60°N–70°N (not shown) as waves deposit their westward momentum, inducing a torque that weakens the stratospheric polar vortex. This is illustrated in Figure 2 by negative stratospheric zonal mean zonal wind anomalies at 60°N. Associated with the stratospheric increase in Z_{PC} and reduced U is an increase in T_{PC} (not shown). The weakened polar vortex causes subsequent upward WAF_Z to refract poleward, as shown by increased WAF_Y near day 60. The poleward WAF_Y is associated with equatorward momentum flux, which leads to deceleration of the zonal wind. In agreement with previous observationally based studies [*Baldwin and Dunkerton*, 2001; *Polvani and Waugh*, 2004; *Cohen et al.*, 2007], this stratospheric circulation response propagates down into the troposphere. By day 70, a negative AO-like response, with high sea-level pressure (P_{SL}) at high latitudes and low P_{SL} at midlatitudes, exists near the surface (not shown).

[21] Several recent papers have shown that the AO response to various thermal forcings, including tropical SSTs (C. J. Fletcher and P. J. Kushner, The role of linear interference in the Annular Mode response to Tropical SST forcing, submitted to *Journal of Climate*, 2010) and EA snow [*Garfinkel and Hartmann*, 2010; *Smith et al.*, 2010], depends on the spatial location of the wave response relative to the stationary background wave (i.e., from the control integration). This is illustrated in Figure 3, which shows the time evolution of the phase (Λ) of WAF_Z and of the control (i.e., low snow) experiment ($WAF_{Z,CNT}$) at 60N and 50 hPa for all-waves and wavenumber-1. The similarity between the all-wave and wavenumber-1 response suggests that the

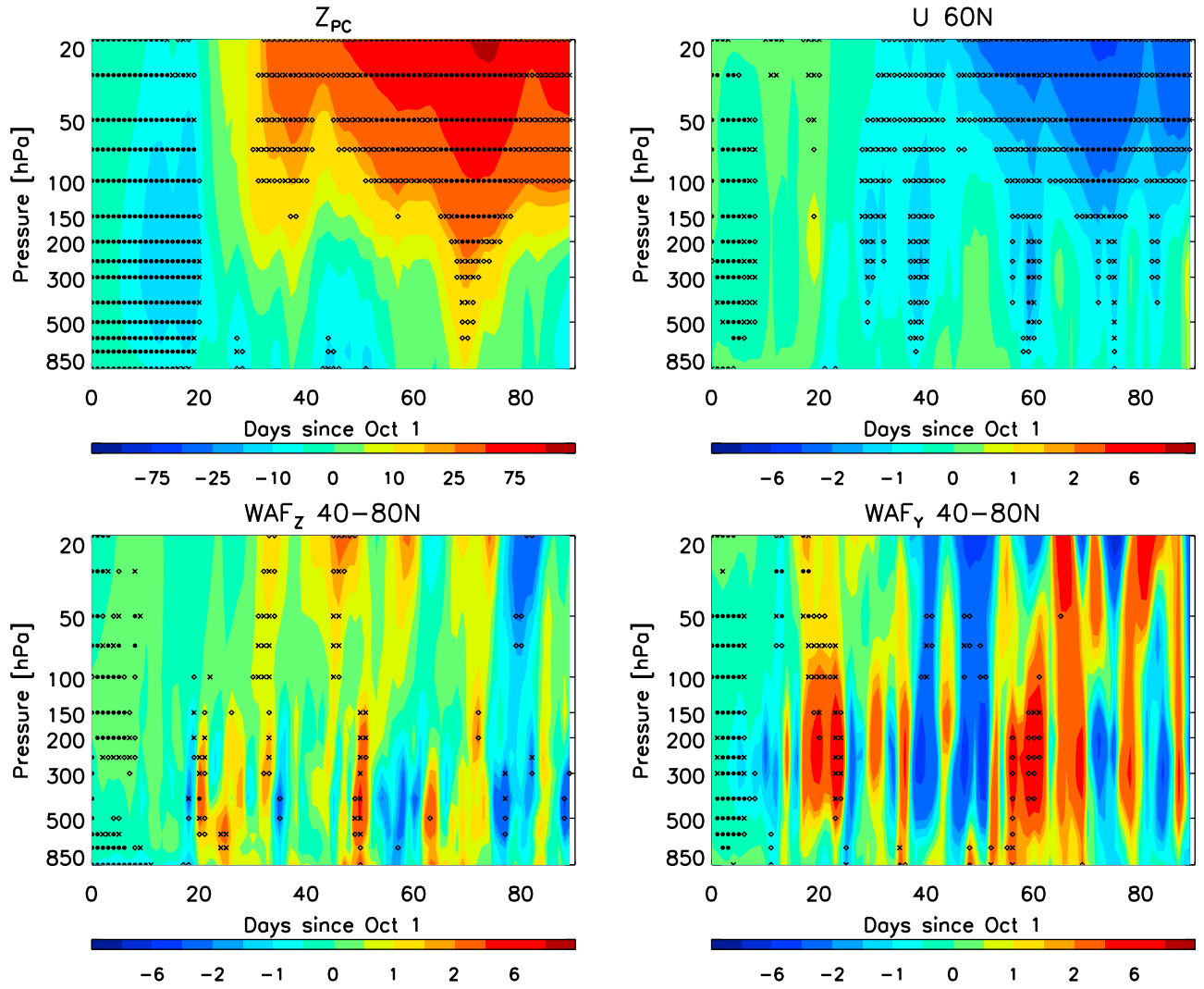

Figure 2. Time-pressure cross sections of the ensemble mean (top left) Z_{PC}, (top right) U 60°N, (bottom left) WAF_Z 40°N–80°N, and (bottom right) WAF_Y 40°N–80°N response to idealized (climatologically high January) EA snow albedo; units are meters, m s^{-1}, 10^{-2} m^2 s^{-2}, and m^2 s^{-2}, respectively. Symbols represent significance as in Figure 1.

wavenumber-1 component dominates the response, similar to *Smith et al.* [2010] (see also section 3.3). As mentioned above, the background wave and response are relatively out of phase (i.e., $90° < \Delta\Lambda \leq 180°$) for the first ~30 days. This leads to destructive interference and negligible propagation of WAF_Z into the stratosphere. During the growth phase (days 30–75), however, both the response and background waves, particularly for wavenumber-1, possess similar phase angles. This is true not only at 50 hPa, where $\Lambda \approx 135°$, but throughout most of the atmosphere, as illustrated by the correspondence of WAF_Z and $WAF_{Z,CNT}$ at 60°N (Figure 3, right). This constructive interference (i.e., $0° \leq \Delta\Lambda < 90°$) is associated with several pulses of upward propagating WAF_Z (which is associated with increased Z_{PC}). During the mature phase (last 15 days), the waves are once again ~180° out of phase, which is associated with a large, negative WAF_Z pulse near day 80.

[22] Linear interference effects were further quantified by calculating the pressure-weighted spatial correlation between WAF_Z and $WAF_{Z,CNT}$ at 60°N (hereafter referred to as r_{WAF}). Table 1 shows that during the growth phase, the all-wave r_{WAF} is 0.50, indicating constructive interference ($r_{WAF} = -0.17$ during the onset phase, indicating destructive interference). We note that an initial negative Z_{PC} response and destructive interference also exists during the first ~30 days in our other experiments.

[23] These results are consistent with other [e.g., *Gong et al.*, 2003a; *Fletcher et al.*, 2009] GCM studies showing a significant snow-AO relationship in response to EA snow forcing over the EA/Siberia region. In particular, the upward propagating Rossby wave response and the magnitude and timing of ΔZ_{PC} closely agree with the results of *Fletcher et al.* [2009], who used the Geophysical Fluid Dynamics Laboratory (GFDL) atmospheric GCM (AM2). The timing and amplitude of our response is also robust to changes in the onset time of the perturbation (i.e., initializing the snow forcing in September or November, rather than October). Furthermore, similar, but weaker, results are obtained with

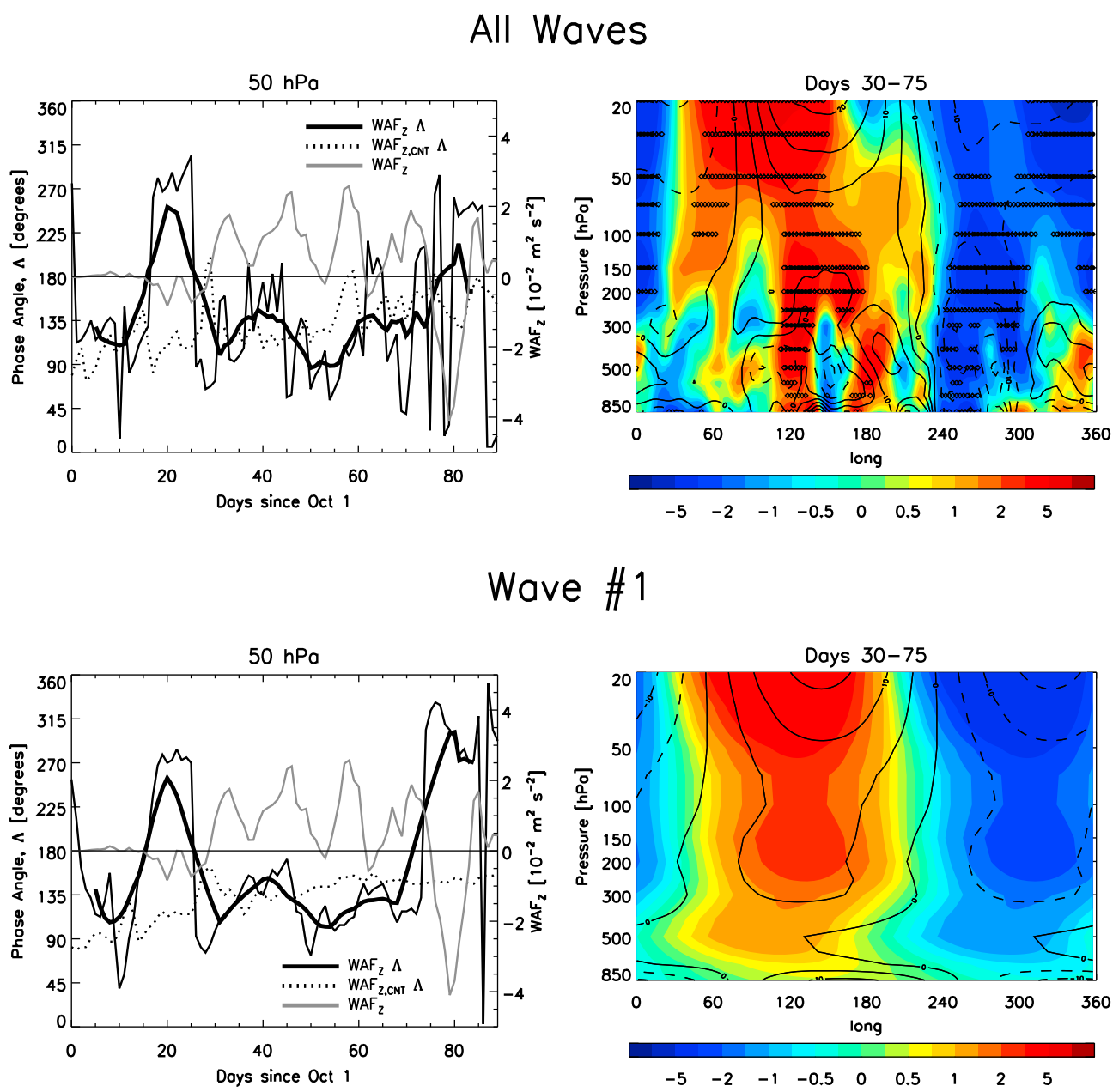

Figure 3. (right) Day 30–75 (i.e., the growth phase) WAF_Z at 60°N for the low-snow control experiment (black lines) and idealized EA response (color shading) for (top) all-waves and (bottom) wavenumber-1. (left) Also included is the time series of the corresponding phase (i.e., longitude of the largest positive WAF_Z) at 50 hPa and 60°N for the control ($WAF_{Z,CNT}$ Λ; black dashed line) and response (WAF_Z Λ; black solid line), and the WAF_Z response (grey). The thick solid black line represents a 10 day running mean of WAF_Z Λ. Symbols in the top right panel represent significance as in Figure 1. Units of WAF_Z are 10^{-2} m^2 s^{-2}. Black contour line in right panels has interval of 5×10^{-2} m^2 s^{-2}, with negative values dashed.

snow forcing over the Siberia region only, as in work by *Fletcher et al.* [2009]. These CAM results add robustness to other GCMs simulated response to snow forcing over the Eurasia/Siberia region.

3.1.2. Realistic Experiments

[24] To simulate more realistic EA (REA) snow forcing, we conduct an additional set of high- and low-snow experiments. Instead of using a perpetual January EA snow cover to simulate anomalously high snow, we use more realistic, seasonally varying values. Using the same 5 years as before (based on the highest five EA October snow covers), October, November and December are each forced with that month's corresponding NOAA-based EA snow cover, averaged over the 5 years. Outside the Eurasian region, snow cover is prescribed using climatologically low snow cover, based on the September snow field from the five lowest EA October snow years (1980, 1987, 1988, 1991, 1994). This high-snow experiment is then compared

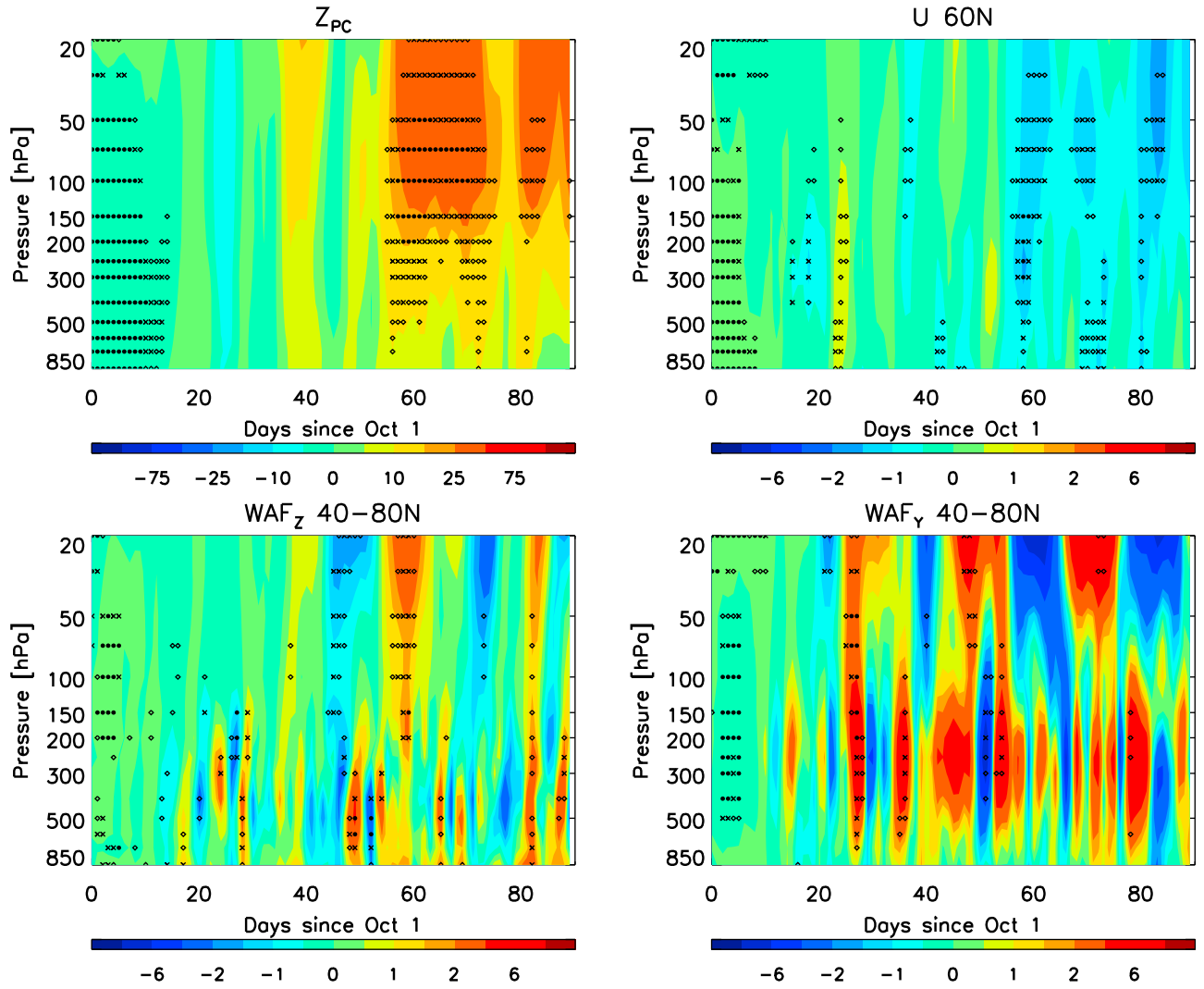

Figure 4. Same as Figure 2 but for realistic (climatologically high October through December) EA snow albedo.

to a low-snow experiment based on perpetual September snow cover using the same five lowest EA October snow years (using the idealized EA low-snow experiment resulted in a similar, but weaker response). This experimental design results in much smaller, but more realistic, seasonal EA albedo changes: 9% for October, 16% for November and 22% for December.

[25] Figure 4 shows the corresponding Z_{PC}, U 60°N and WAF response. Similar to the idealized EA experiment, an upward stratospheric WAF_Z pulse and positive Z_{PC} anomaly develops in response to the snow forced EA surface cooling. This response, however, is delayed until day ~40 and is quickly followed by a large decrease in WAF_Z. A significant response does not emerge until day 60, when a strong WAF_Z pulse propagates into the stratosphere and initiates changes in the stratospheric circulation similar to IEA, including increased geopotential heights and decreased zonal winds near 60°N. These anomalies then propagate down through the troposphere for the remainder of the simulation, yielding a surface negative AO-like response.

[26] Figure 5 shows the corresponding changes in December Z 500 hPa and P_{SL}. Similar to the negative phase of the AO, EA snow forcing yields increases in high-latitude tropospheric geopotential height and sea-level pressure, and decreases in both quantities in the midlatitudes. The increase in P_{SL} near Siberia is a direct, local result of the snow forcing, as in work by *Fletcher et al.* [2009]. Attempts at simulating even more realistic EA snow forcing, by using the five largest (smallest) EA snow covers of each month, October, November, and December, for the high- (low-) snow experiment, yielded a significantly weaker snow-AO relationship (not shown).

3.1.3. Comparing IEA and REA

[27] Although there appears to be several significant differences in the response to idealized EA (IEA) versus realistic EA (REA) snow, most of these differences are related to sampling effects. For example, the strong REA WAF_Z response near day 60, which is stronger than any of the IEA pulses, occurs in a 50-member IEA subset. The REA response, however, exhibits much larger variability (which is consistent with the smaller forcing and greater noise to

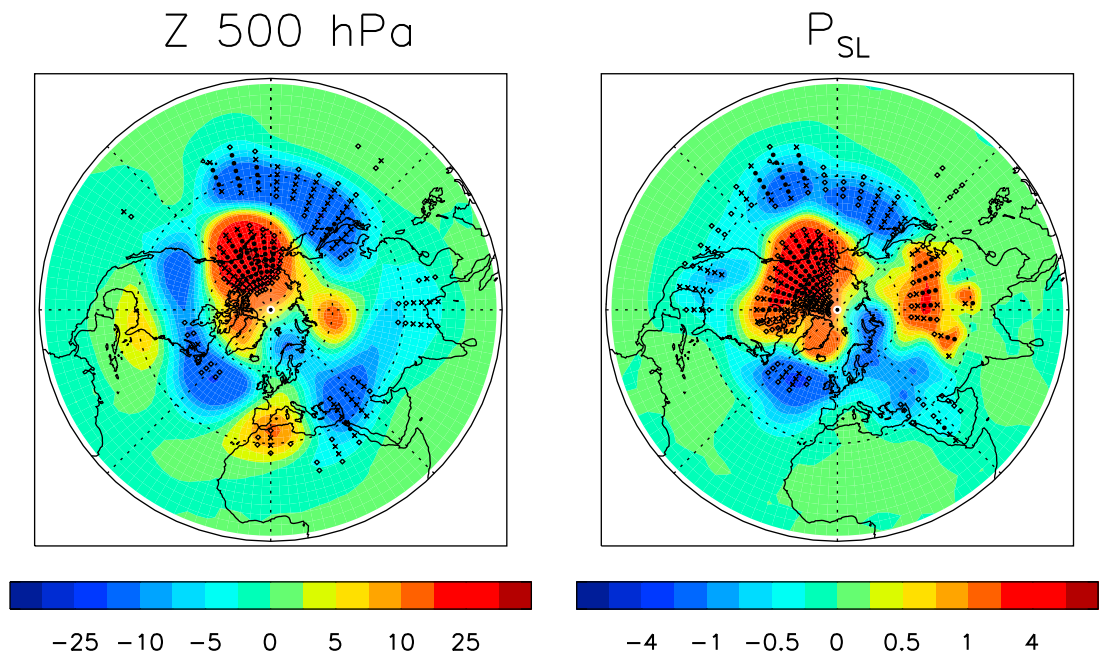

Figure 5. December ensemble mean response to realistic EA snow albedo forcing showing the change in (left) Z 500 hPa and (right) P_{SL}; units are meters and hPa, respectively. Symbols represent significance as in Figure 1.

signal ratio). An even stronger REA WAF_Z pulse occurs for ensemble members 1–50; this is in contrast to a very weak WAF_Z response for ensemble members 51–100 (not shown). These sampling differences, however, are consistent with linear interference effects. Table 1 shows that the REA r_{WAF} over the growth phase (days 40–89) for all-waves is 0.41 for ensemble members 1–50, but only 0.04 for members 51–100. This difference in the interference correlation is due to changes in the spatial position of the wave response, as opposed to the climatological wave. The corresponding correlation for the two 50-member IEA subsets is similar at 0.25 and 0.34. The stronger troposphere-stratosphere coupling for the REA experiment also appears to be related to sampling. Consistent with the weaker WAF_Z response for ensemble members 51–100, a significantly weaker and less persistent near-surface Z_{PC} response also exists (not shown). However, the ratio of the Z_{PC} response in the troposphere, relative to that in the stratosphere, is still larger for REA.

[28] The remaining difference between the two EA experiments is a weaker, delayed stratospheric Z_{PC} response to REA snow forcing that couples more quickly to the troposphere. The delayed Z_{PC} response is consistent with initial destructive wave interference that lasts longer. The REA all-wave $r_{WAF} = -0.29$ during the onset phase, which spans the first ~40 days, as opposed to the first ~30 days for IEA. The weaker response is due to the smaller REA thermal forcing, and weaker constructive wave interference during the growth phase (Table 1). This is particularly true for wavenumber-1, which for IEA possesses the largest amplitude (see section 3.3), and determines the overall character of the response.

3.2. North America

[29] Similar to the idealized EA experiment, we conduct analogous idealized experiments for the North American region, defined as 30°N–90°N and 188°E–300°E. The NA high-snow experiment features January-based snow albedo using the same 5 years of NOAA snow cover fraction data as in the EA experiments; the NA low-snow experiment features perpetual September-based SA, also derived from the same 5 years of NOAA f_{snow}. Thus, we do not explicitly use the five largest NA January snow years; however, this should make little difference since the snow forcing is already exaggerated (i.e., using a January snow albedo in early autumn represents an above normal snow). Because of the delayed circulation response to NA snow forcing, these experiments are integrated for one additional month, October through January.

[30] Figure 6 shows the October ensemble mean albedo response ($\Delta\alpha$ = 21%, similar to that for the idealized EA experiment), which results in a decrease in the net surface solar radiation of −14.9 W m^{-2} and a NA surface cooling of −0.73 K. Although this surface cooling is 40% smaller than that for the idealized EA experiment, it is 30% larger on a per forcing area basis. Figure 6 also shows the surface temperature change for December. Not only does NA possess significant surface cooling, but eastern Eurasia does as well. Averaged over Siberia (30°N–60°N; 35°E–135°E), the December ΔT_{sfc} is −0.40 K, more than 50% of the imposed surface cooling over NA. This cooling over Siberia, where there is no snow forcing, suggests NA snow cover can also induce a remote climate response.

3.2.1. Transient Response

[31] Figure 7 shows NA time-pressure cross sections of the response in Z_{PC}, U 60°N and the wave activity flux. Unlike prior GCM North American snow studies [*Gong et al.*, 2003b; *Sobolowski et al.*, 2010], NA snow forcing results in a significant snow-AO relationship, with qualities similar to that based on anomalous Eurasian snow cover, particularly in the stratosphere/upper troposphere. During

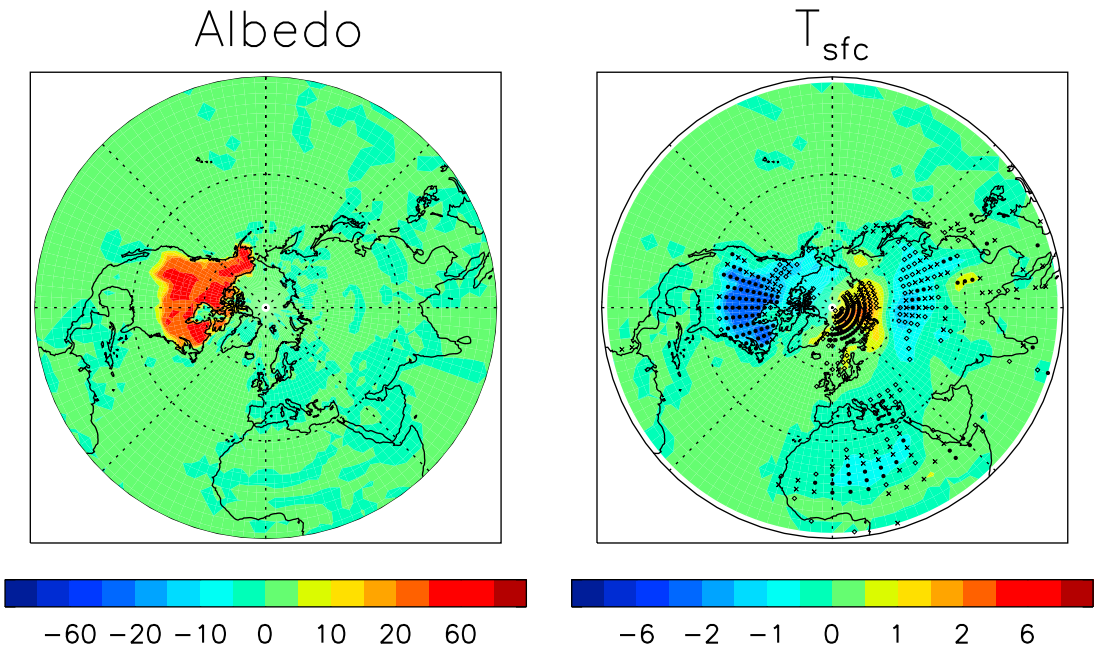

Figure 6. October ensemble mean NA (30°N–90°N and 188°E–300°E) (left) snow albedo forcing and (right) December surface temperature response. NA OCT mean $\Delta\alpha = 21\%$; $\Delta T_{sfc} = -0.73$ K. Symbols for ΔT_{sfc} represent significance as in Figure 1.

the growth phase (days 60–85), a significant tropospheric WAF_Z pulse occurs, which subsequently propagates up into the stratosphere near day 80. These waves converge, as represented by decreased northward transport of quasi-geostrophic potential vorticity (not shown), depositing their westward momentum and weakening the stratospheric polar vortex (i.e., U 60°N). This is associated with increased Z_{PC}, which propagates down through the upper troposphere/midtroposphere, albeit weak and not significant at the 90% confidence level. Similar to the EA forcing experiments, this WAF_Z response is centered over the Siberia region (not shown), corresponding to the area of remote surface cooling in Figure 6.

[32] This stratospheric/upper tropospheric negative AO-like response, and the corresponding WAF_Z pulse, are short-lived, however. After the main WAF_Z pulse near day 80, downward WAF_Z dominates, with a large negative pulse near day 110. Furthermore, a significant enhancement of the prevailing equatorward tropospheric wave activity occurs, as shown by the negative ΔWAF_Y (Figure 7). This response is associated with a poleward flux of momentum and wave divergence (not shown), which results in increased U 60N. To maintain geostrophic and hydrostatic balance, a midlatitude meridional overturning circulation is generated in the troposphere (not shown), with northerly (southerly) surface (midtropospheric/upper tropospheric) flow and rising (sinking) air poleward of 60°N (30°N–60°N). The rising air is associated with adiabatic expansion and cooling, while the sinking air compresses and warms, yielding an increase in latitudinal temperature gradient consistent with the increased zonal mean westerlies near 60°N. As shown in Figure 8, these effects are more apparent in the sea-level pressure field, as a decrease in Arctic P_{SL} and an increase in midlatitude P_{SL}. This positive, tropospheric AO mode response to NA snow forcing agrees with *Gong et al.* [2003b]. For comparison, we also include the stratospheric negative AO response for December (i.e., Z_{PC} at 100 hPa), which features nearly the opposite pattern.

[33] Similar, but weaker results are obtained when the NA snow forcing is varied (e.g., perpetual December snow albedo). Furthermore, more realistic NA snow forcing (i.e., SA prescribed similar to the more realistic EA scenario and integrated through February) also yields similar results; however, the Siberian WAF_Z pulse and the subsequent increase in stratospheric Z_{PC} is delayed until day 115 (late January), likely due to the smaller fall forcing. The tropospheric positive AO response also occurs, in mid-February. The mechanisms associated with this negative AO signal are discussed in section 3.2.2.

3.2.2. Transient Eddy Response

[34] Figure 9 shows time series of ΔT_{sfc} averaged over midlatitude NA (30°N–60°N; 188°E–300°E) and Siberia (30°N–60°N; 35°E–135°E), and poleward of 60°N (i.e., the polar cap) for the idealized NA snow experiment. Also shown is ΔZ_{PC} and ΔWAF_Z 40°N–80°N at 100 hPa. The initial response to NA snow forcing is a decrease in T_{sfc-NA} of ~0.9 K, which persists, although weakening somewhat, throughout the integration time period. A small, but significant decrease in both Z_{PC} and T_{sfc-PC} also occurs during the first ~20 days, after which mostly nonsignificant changes in all quantities (except T_{sfc-NA}) exist for the next ~40 days. Beginning in December, near day 60, T_{sfc-SB} begins to decrease, reaching a minimum of nearly −1 K near day 75. This midlatitude Siberian cooling precedes increases in Z_{PC}, T_{sfc-PC} and WAF_Z. This suggests that anomalous NA SA causes a remote climate response that occurs in two phases.

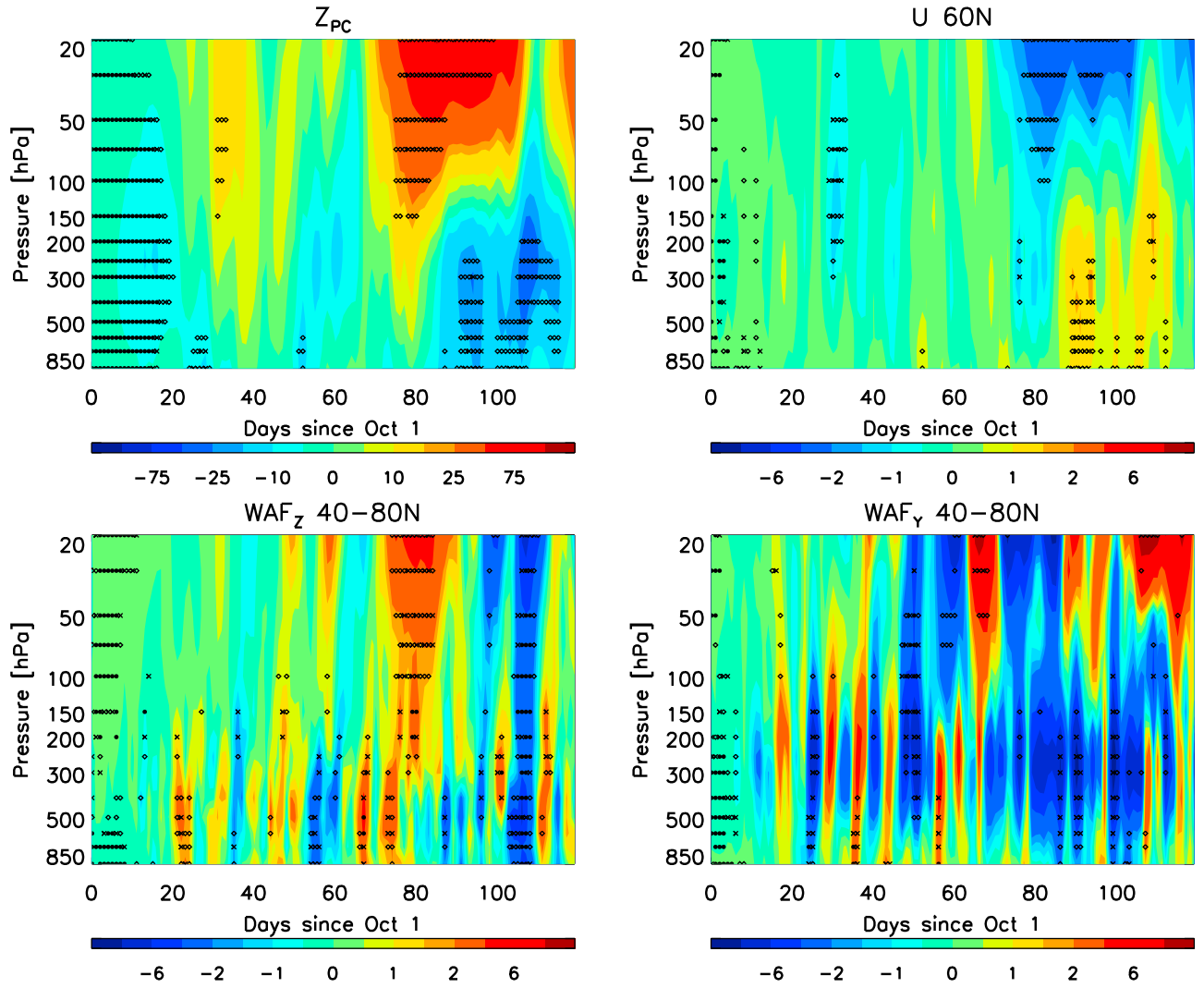

Figure 7. Same as Figure 2 but for NA snow forcing and extending through January.

First, NA snow cover results in significant Siberian surface cooling, that extends through the troposphere. This cooling then triggers a WAF$_Z$ pulse over the Siberian region, that propagates into the stratosphere and alters stratospheric circulation (e.g., increases Z_{PC}), which then propagates back down through the upper troposphere/midtroposphere. Due to destructive interference between WAF$_Z$ and WAF$_{Z,CNT}$ past day 89 (r_{WAF} = −0.12 for all-waves and −0.50 for wavenumber-1), however, the WAF$_Z$ response is too short-lived to produce negative AO-like changes at the surface, which remain confined to the stratosphere/upper troposphere.

[35] A remaining question exists: how does the NA snow forcing induce remote cooling over Eurasia? Although there is a 0.7% increase in Siberian snow cover fraction (f_{snow}) and a 0.19 cm increase in snow depth during December (not shown), the nonalbedo effects of a small increase in f_{snow} are likely not the cause of the relatively large Siberian December surface cooling. For example, the decrease in T_{sfc} over NA, where the albedo effects of a much larger snow perturbation are specified (Δf_{snow} based on the NOAA data is 33.2%), is very similar to the December Siberian surface cooling. During late November and early December, the NA surface cooling is actually smaller (Figure 9). Moreover, the Siberian snow response is shifted a few days later than ΔT_{sfc-SB} (not shown), which indicates the snow is responding to the decrease in temperature (as for the idealized EA experiment), and not the other way around.

[36] Given the dependence of midlatitude transient eddies on temperature gradient and baroclinicity, a large, sustained thermal forcing as represented by anomalous NA snow cover may induce a transient response. Similar to *Sobolowski et al.* [2010], we therefore investigate the role transient eddies play in the EA response to NA snow forcing. To isolate activity on a 2–8 day time scale, a high-pass filter is applied to the daily departures from the monthly means of the relevant variables (e.g., v, u, T) before computing transient eddy statistics [*Trenberth*, 1991]. Figure 10 shows the ensemble mean change in the 500 hPa geopotential height variance $(\overline{Z'^2})^{0.5}$ for October and mid-November to mid-December. The initial response is an increase in transient eddy activity over the NA snow forcing region, consistent

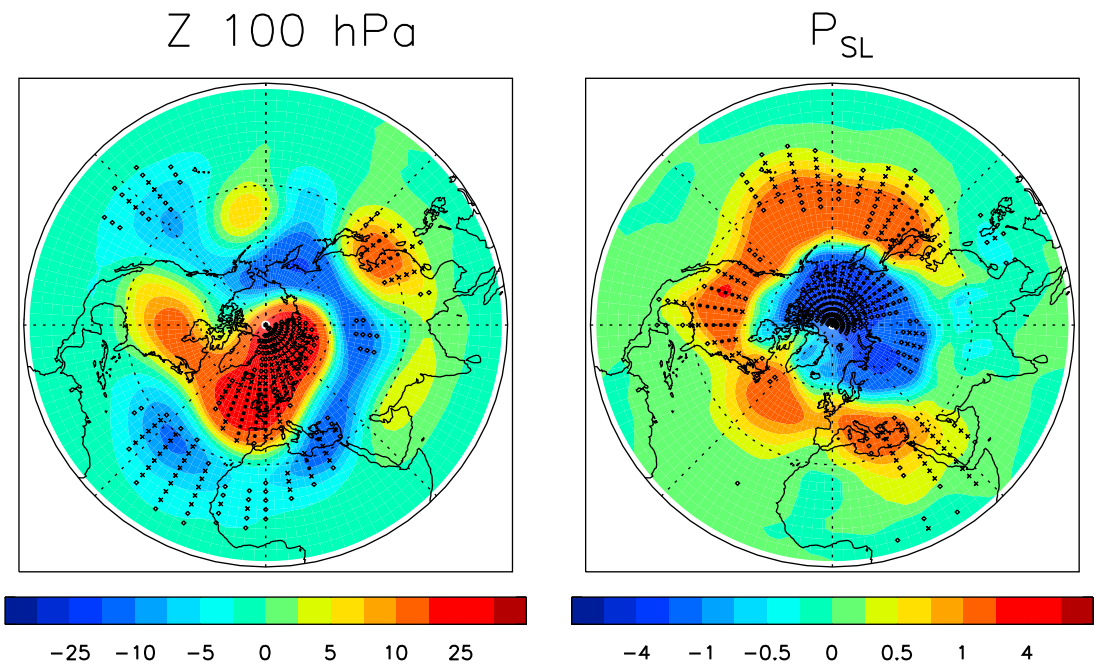

Figure 8. Ensemble mean response to NA snow albedo forcing showing (left) Z 100 hPa for December and (right) P_{SL} for January; units are m and hPa, respectively. Symbols represent significance as in Figure 1.

with the increased temperature gradient/baroclinicity created by the NA surface cooling. This increase is maintained (but less significant) through late fall over NA; however, mid-November to mid-December also features several significant areas of reduced transient eddy activity downstream of NA, over the Atlantic Ocean and into Europe and northern Siberia, which is opposite to findings by *Sobolowski et al.* [2010].

[37] Figure 11 shows the mid-November to mid-December response of four additional measures of transient eddy/storm

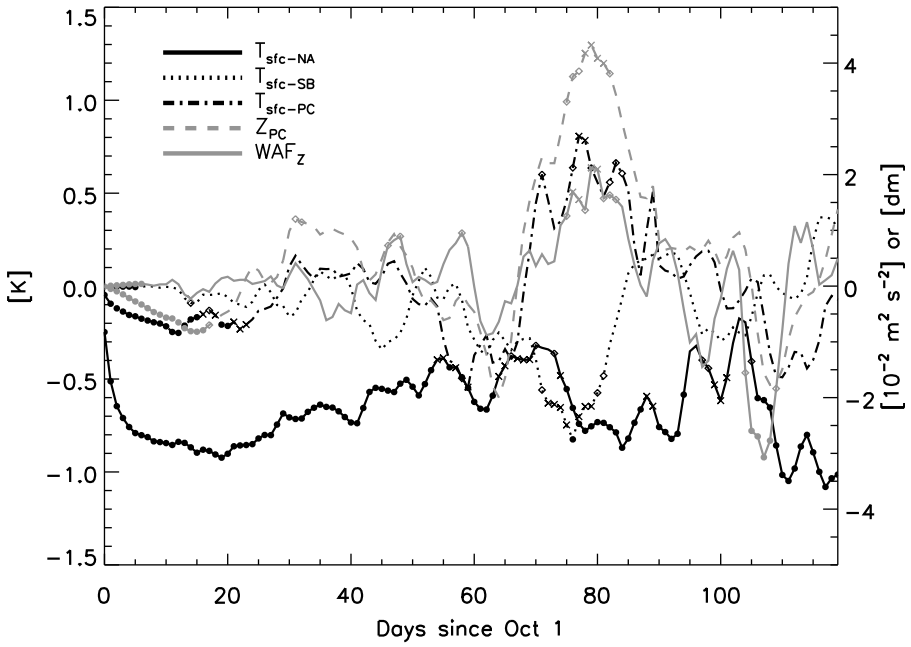

Figure 9. Transient response to NA snow forcing showing (left axis) T_{sfc} over midlatitude Siberia (30°N–60°N; 35°E–135°E) and North America (30°N–60°N; 188°E–300°E), and the polar cap (>60°N). Also shown is (right axis) Z_{PC} and WAF_Z 40°N–80°N, both at 100 hPa. Symbols represent significance at the 90% (diamond), 95% (cross), and 99% (dot) confidence level. Units are K for temperature variables, decimeters (dm) for Z_{PC}, and 10^{-2} m^2 s^{-2} for WAF_Z.

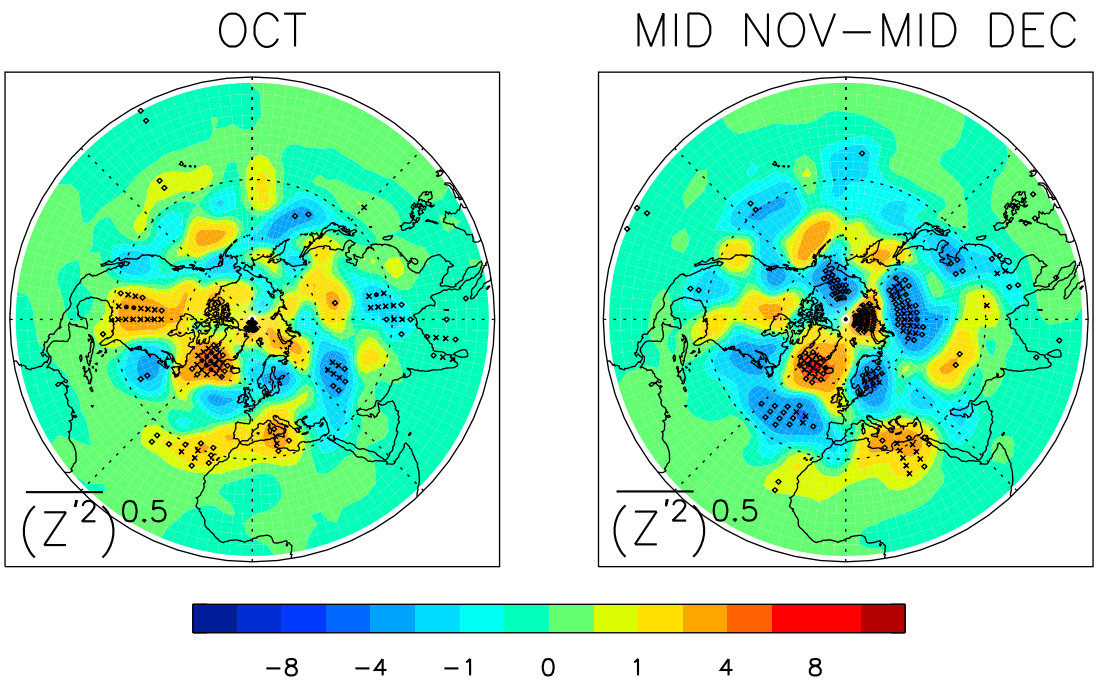

Figure 10. The 500 hPa geopotential height variance $(\overline{Z'^2})^{0.5}$ response for NA snow forcing during (left) October and (right) 15 November to 15 December. Units are meters.

track activity. Eddy kinetic energy (EKE) is written as [*Rind et al.*, 2005b]

$$EKE = 0.5\overline{(u'^2 + v'^2)}. \quad (3)$$

Over the North Atlantic, Europe and much of Asia, the negative EKE 500 hPa response suggests a decrease in the transfer of available eddy potential energy to eddy kinetic energy. Similarly, 850 hPa poleward $\overline{v'T'}$ and 500 hPa poleward $\overline{u'v'}$ temperature and momentum eddy fluxes decrease over many of the same regions. The decreased poleward flux of heat and momentum suggest that these regions should also experience decreased baroclinic growth. The baroclinic growth is estimated according to the maximum Eady growth rate (EGR) [*Lindzen and Farrell*, 1980]

$$EGR = -0.3125\frac{g}{NT}\frac{\partial T}{\partial y}, \quad (4)$$

where N is the Brunt-Vaisala frequency. Figure 11 shows the ΔEGR 500 hPa is negative over much of northern Europe and Siberia, suggesting decreased baroclinicity.

[38] The general agreement between these measures of transient eddy activity suggest that during late November/early December, storm track activity is weakened downstream of NA and into Eurasia. The reduced poleward $\overline{v'T'}$ over Europe and much of Siberia implies a decrease in the northward flux of warm air. This is consistent with the early/mid-December Siberian cooling (Figure 9), which subsequently triggers the vertically propagating WAF_Z pulse. The downstream weakening of transient eddies, however, is not sustained after mid-December. In particular the reduced $\Delta\overline{v'T'}$ over Siberia no longer exists (not shown), consistent with the short-lived nature of the Siberian cooling (Figure 9).

3.3. Northern Hemisphere

[39] Our results based on EA and NA snow forcing yield a conflicting picture of the snow-AO relationship. Anomalous EA snow albedo yields a negative AO-like response that extends from the stratosphere to surface; anomalous NA SA, however, eventually yields a positive tropospheric AO, after an initial negative AO-like response confined to the stratosphere/upper troposphere. In the real world, both NA and EA simultaneously possess snow cover. If EA and NA both possess high snow cover in a given autumn, what is the subsequent wintertime climate response? Given the larger surface area of EA, does the EA snow-AO relationship dominate; if so, how does NA snow cover affect the response?

[40] Our final experiment investigates the atmospheric circulation response to snow forcing over the entire Northern Hemisphere (NH) poleward of 30°N. As with the idealized EA and NA experiments, we perform a high-snow experiment based on NOAA snow cover fraction data for January, averaged over the same 5 years; the NH low-snow experiment features perpetual September-based snow albedo forcing. The prescribed NH snow forcing is therefore approximately equal to the sum of the idealized EA and NA snow forcing. However, as we will show, the sum of the EA and NA responses does not resemble the NH response, suggesting the interaction between NA and EA, for our forcing details, is nonlinear.

[41] Figure 12 shows the changes in Z_{PC}, U 60N and WAF. Despite the fact EA snow forcing, as well as NA snow forcing, both yield significant Z_{PC} and U 60N responses, the sum of the two do not. The increase (decrease) in stratospheric Z_{PC} (U 60°N) is smaller than that for EA and NA, nor is it very significant. Furthermore,

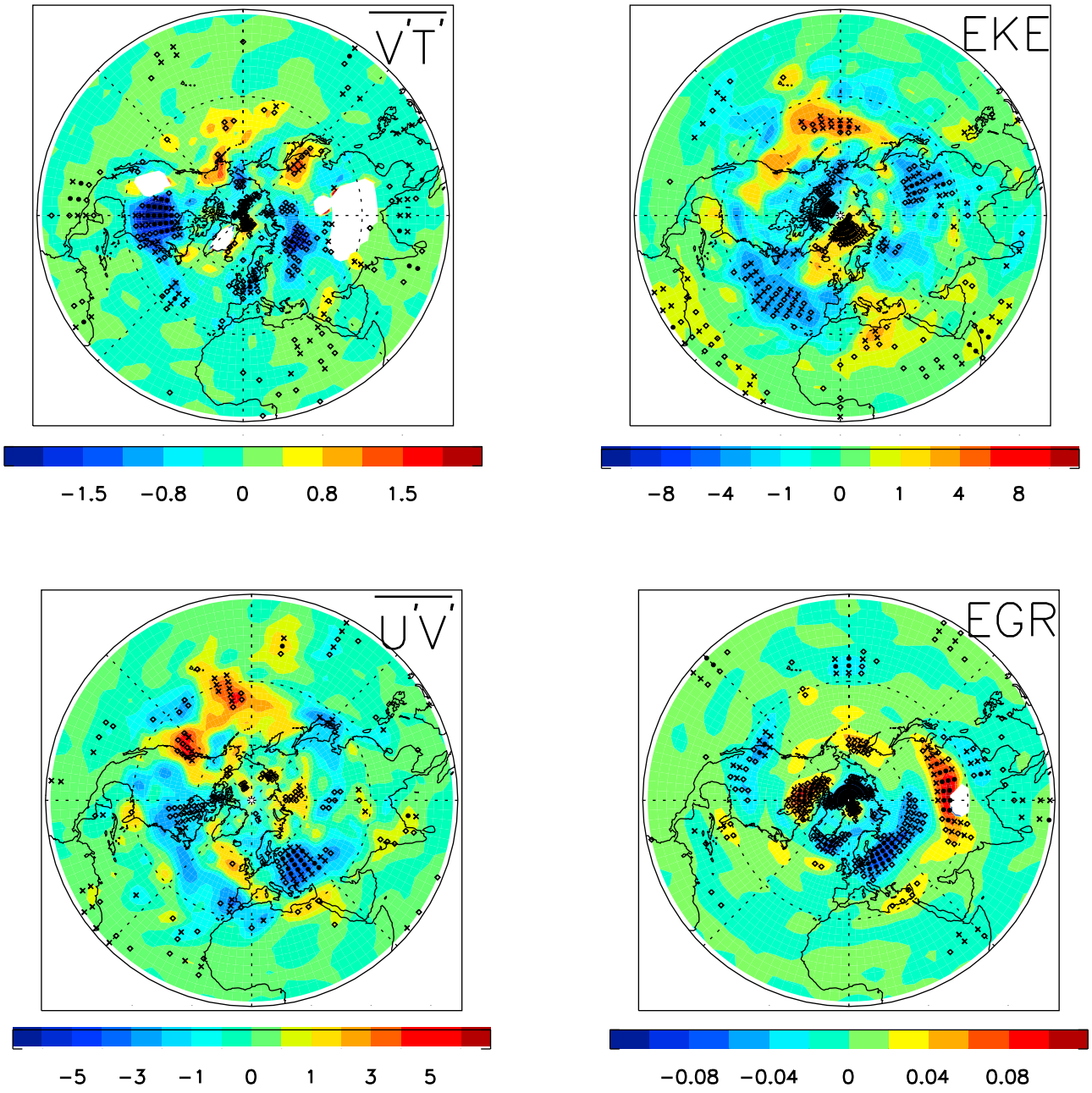

Figure 11. The 15 November to 15 December transient activity response to NA snow forcing showing the (top left) 850 hPa meridional temperature flux, $\overline{v'T'}$, (top right) 500 hPa eddy kinetic energy, EKE, (bottom left) 500 hPa northward momentum flux, $\overline{u'v'}$, and (bottom right) 500 hPa maximum Eady growth rate, EGR; units are K m s^{-1}, m^2 s^{-2}, m^2 s^{-2}, and day^{-1}, respectively.

similar to NA snow forcing, the stratospheric circulation anomalies are unable to propagate down through the troposphere. This weakened wave-mean flow interaction is consistent with ΔWAF_Z. Despite several significant tropospheric WAF_Z pulses, very little propagates into the stratosphere.

[42] Figure 13 shows the sums of WAF_Z at 50 hPa and the northward transport of quasigeostrophic potential vorticity ($\Sigma\overline{v'q'}$) at 20 hPa for the three idealized experiments. The cumulative WAF_Z, as opposed to individual pulses, has been shown to correlate better to the surface AO [*Polvani and Waugh*, 2004]. Consistent with this, ΣWAF_Z for the NH shows very little cumulative increase, particularly past day 60, relative to the other two experiments. Similarly, NH $\Sigma\overline{v'q'}$ shows little cumulative decrease, indicating negligible wave convergence. This result suggests NA and EA snow cover destructively interfere with one another and that anomalous NH snow cover yields a significantly muted snow-AO relationship.

[43] Figure 14 shows the Fourier decomposition of WAF_Z 60°N into individual wavenumber components for the IEA, NA and NH experiments (averaged over each region's growth phase). As mentioned in section 3.1.1,

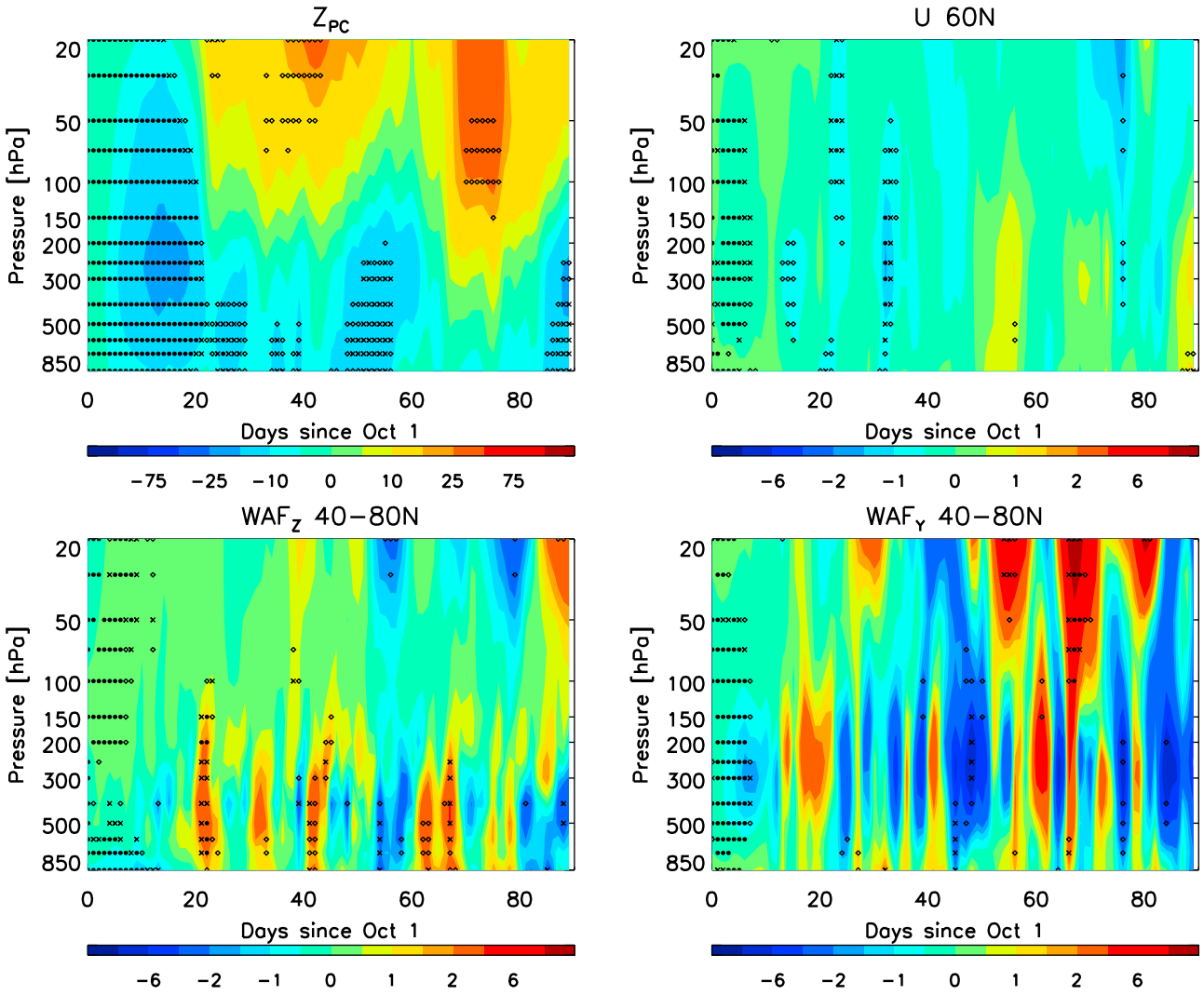

Figure 12. Same as Figure 2 but for NH snow forcing.

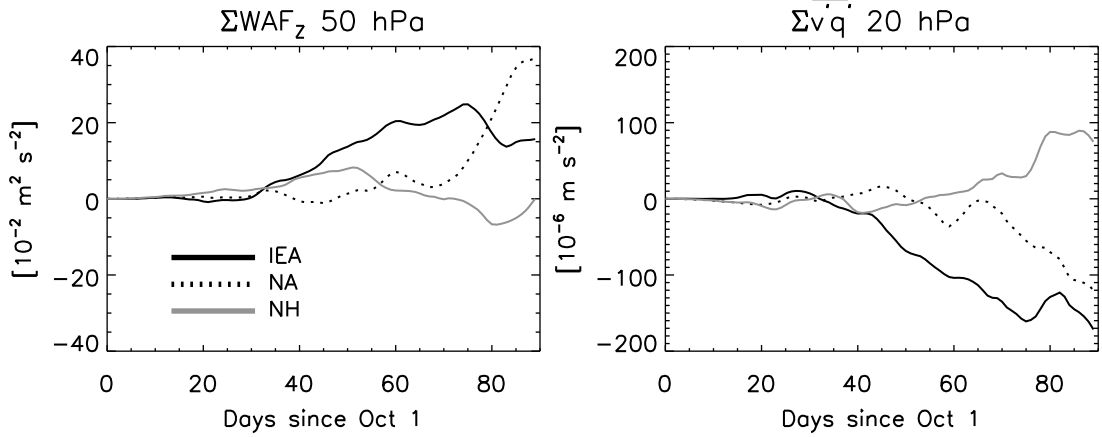

Figure 13. Transient response to IEA, NA, and NH snow forcing showing (left) ΣWAF$_Z$ 40°N–80°N at 50 hPa and (right) Σ $\overline{v'q'}$ 40°N–80°N at 20 hPa.

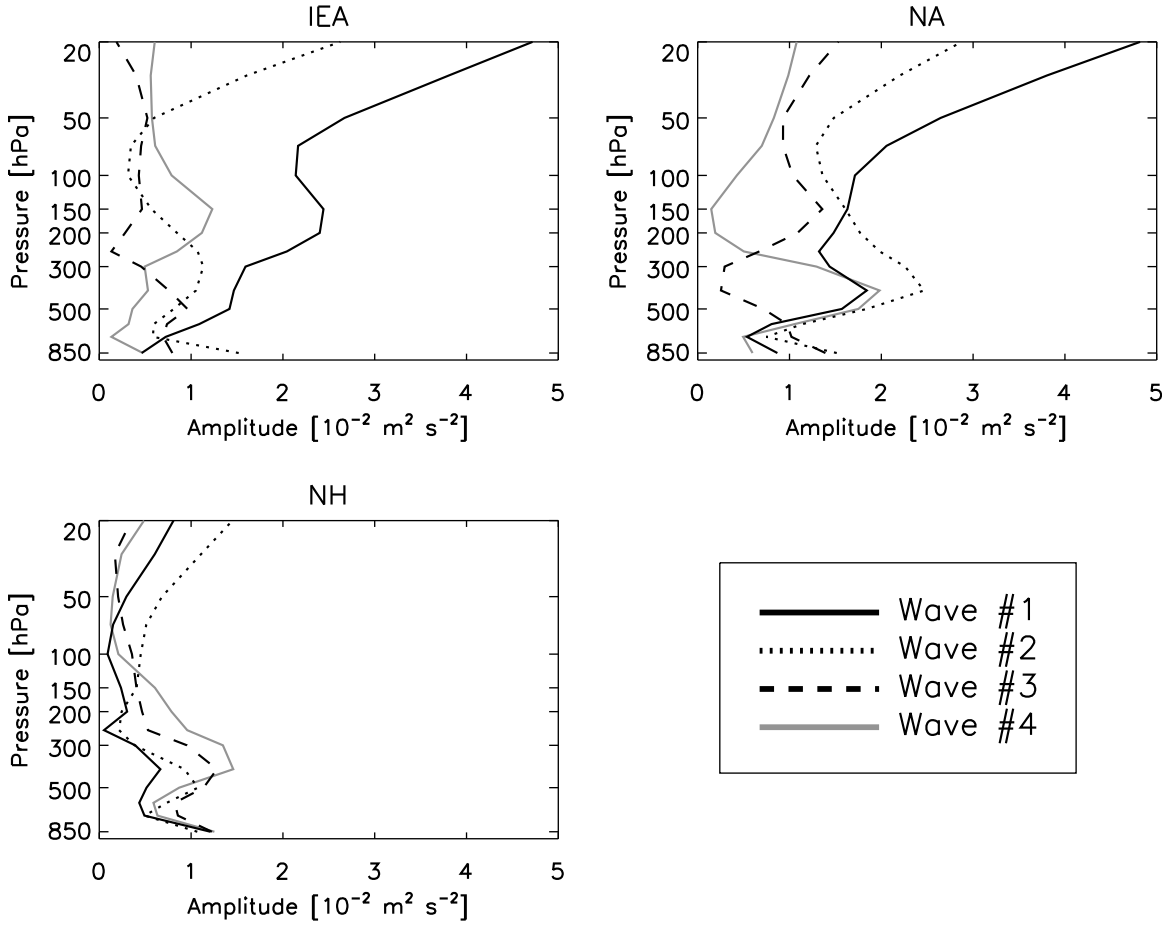

Figure 14. Fourier decomposition into individual wavenumber components of WAF_Z averaged over the growth phase (days 30–75 for IEA and NH; days 60–85 for NA) at 60°N for idealized (top left) Eurasia, (top right) North America, and (bottom left) Northern Hemisphere experiments.

the IEA tropospheric WAF_Z is comprised primarily of wavenumber-1, which is also dominant, in addition to wavenumber-2, in the stratosphere. This is similar for NA, except a larger contribution comes from wavenumber-2. For NH, however, wavenumber-1, and to a lesser extent wavenumber-2, is significantly muted. Table 1 shows that the NH pressure-weighted spatial correlation between WAF_Z and $WAF_{Z,CNT}$ is −0.09 for all-waves, −0.24 for wavenumber-1 and −0.81 for wavenumber-2. Therefore, the NH experiment features destructive wave interference, particularly for the important wavenumbers-1 and -2, that dominates throughout the 90 day integration. This results in negligible propagation of WAF into the stratosphere and a muted AO response.

4. Discussion

[44] As mentioned in section 1, several observational studies have shown significant correlations between autumn EA snow cover and the following winter's AO. Despite the significance of these correlations, the magnitude is about 0.5 [*Cohen et al.*, 2007; *Hardiman et al.*, 2008], leading some to question the robustness of the association [e.g., *Kushnir et al.*, 2006]. The preceding modeling results suggest (1) anomalous NA and EA snow cover force opposite phases of the AO, with EA (NA) snow forcing a negative (positive) surface AO, and (2) NH snow yields a dampened snow-AO response. Therefore, the EA snow-AO correlation may be muted during those years when both EA and NA snow cover is anomalously high. Using monthly NCEP/NCAR Reanalysis data from 1972–2006, however, suggests that this is not the case. The correlation (after detrending both time series) between EA SON snow cover (from the NOAA satellite data) and the DJF surface AO is −0.46. Recalculating this correlation, after removing those years with simultaneously high EA and NA snow cover yields little improvement. The relationship actually weakens to −0.36 when the 10 largest NA and EA snow years in common are excluded. This is robust to other metrics, including October snow, excluding the five largest NA and EA snow years in common, etc.

[45] The NA and EA CAM experiments also suggest a difference in the timing of the AO response, with the EA snow-AO response preceding the corresponding NA response. Thus, EA and NA snow may not interfere with one another, if the EA negative AO response occurs far enough in advance of the NA positive AO response. Figure 15, which shows the correlation between EA and NA SON snow cover and the AO from November through the following April, supports this argument. EA snow is associated with an AO

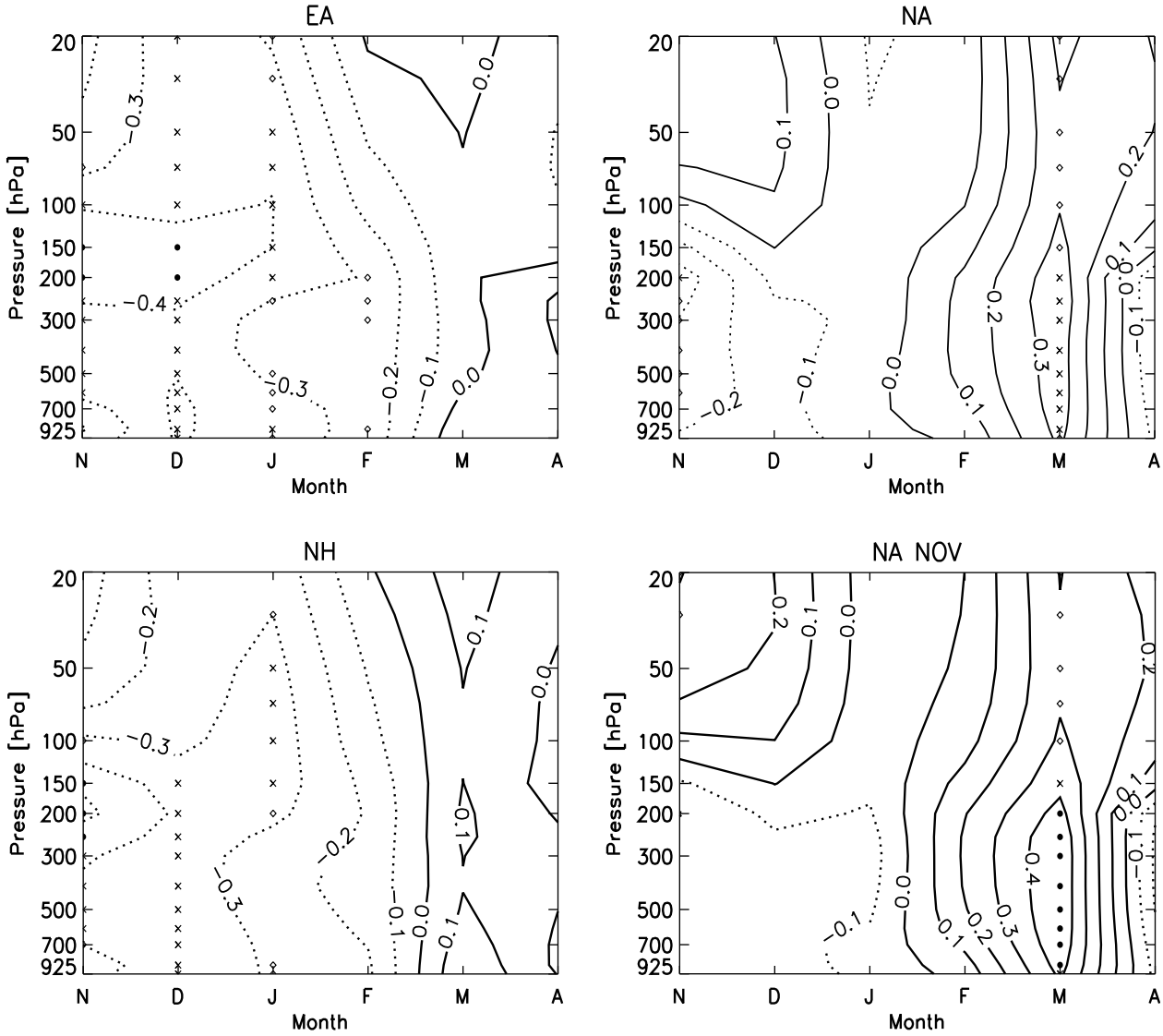

Figure 15. NCEP/NCAR Reanalysis lag correlations between (top left) Eurasian, (top right) North American, and (bottom left) Northern Hemisphere SON snow cover and the AO for November through the subsequent April. (bottom right) Also included is the corresponding North American correlation using November snow. The AO is calculated as the leading principal component of geopotential heights poleward of 20°N, separately for each pressure level. Symbols represent significance as in Figure 1. Negative correlations are dashed lines.

response during DJF, whereas NA snow is associated with an AO response, of the opposite sign, in March. Furthermore, the NA snow-March AO correlation is largest in the troposphere (0.31 at the surface), in agreement with the CAM experiments (the winter stratospheric correlations are also negative, as with CAM, but small and not significant). Figure 15 also shows that the NA-AO relationship is stronger using November snow. Here, all tropospheric correlations increase to >0.4 and are significant at the 99% confidence level. A similar significant relationship also exists for the NAO (not shown), estimated as by *Hurrell et al.* [2004] as the difference in geopotential heights averaged over a southern (30°N–50°N; 80°W–20°E) minus a northern (60°N–80°N; 80°W–20°W) domain.

[46] Figure 15 also includes the corresponding correlations based on NH snow cover. Similar to the CAM results, NH snow cover yields a snow-AO response similar to, but weaker than, that based on EA snow alone. At the surface, the DJF AO-SON NH snow correlation is −0.39, compared to −0.46 for EA SON snow alone. The CAM NH response, however, is much weaker than observations. Note also the small positive correlations in March, due to NA snow cover.

[47] To our knowledge, this is the first study combining a GCM and observations to show NA, in addition to EA, snow yields a remote AO response. Moreover, several features of the NA snow-AO relationship are consistent between these CAM experiments and NCEP/NCAR Reanalysis, including the sign of the relationship, its tropospheric maximum, and its delayed, late-season development. Although the CAM

experiments only yield qualitative information on the actual timing of the response, Figure 15 shows that the NA and EA AO responses are offset by 1–2 months, with EA snow forcing a negative AO in early winter/midwinter and NA snow forcing a positive AO, primarily in the troposphere, in late winter/early spring. We are currently conducting additional research to investigate these findings, especially the NA results, which are the most novel.

5. Conclusions

[48] We conduct three primary experiments, investigating the effects of idealized, but realistic snow anomalies on NH atmospheric circulation, emphasizing remote, AO-like responses. For each experiment, a pair of 100 ensemble members are integrated through the fall–early winter season, using independent initial conditions. The first set of branch runs features a climatologically high snow albedo (SA); the second set features climatologically low SA. Anomalous Eurasian snow albedo in autumn results in increased vertically propagating wave activity that penetrates into the stratosphere and produces a negative stratospheric AO. This stratospheric response subsequently propagates down through the troposphere, resulting in a similar, negative AO signal at the surface in mid-December. This result is robust to the onset of the perturbation and to several different EA snow forcings, including more realistic, seasonally varying values. This response is consistent with observations [e.g., *Cohen et al.*, 2007] and non-CAM GCM Eurasian/Siberian snow experiments based on prescribed snow mass using GFDL AM2 [*Fletcher et al.*, 2009] and European Centre Hamburg Atmospheric Model 3 (ECHAM3) [*Gong et al.*, 2003a]. Consistency between multiple GCMs is an important result because model details, such as stratospheric representation and orographic gravity wave drag parameterization, have been shown to significantly affect tropospheric-stratospheric coupling, as well as the snow-AO relationship [*Sigmond et al.*, 2008; *Fletcher et al.*, 2009; *Shaw et al.*, 2009]. Our results also show that increased albedo is the primary mechanism by which snow affects atmospheric circulation, as suggested by *Fletcher et al.* [2009].

[49] Similar experiments using North American SA anomalies are also performed. Prior GCM NA snow experiments have yielded inconsistent results, ranging from positive AO/NAO-like tropospheric responses [*Gong et al.*, 2003b; *Klingaman et al.*, 2008] to negligible AO-like changes and Eurasian springtime warming [*Sobolowski et al.*, 2010]. In this study, we find that NA snow anomalies are able to produce a negative AO-like mode similar to that based on EA snow forcing, but weaker, shorter-lived, and confined to the stratosphere/upper troposphere; this response eventually gives way to a tropospheric AO signal of the opposite phase. The first part of the NA response involves weakening of transient eddies downstream of NA, extending across the North Atlantic and into Eurasia. This response is associated with decreased eddy kinetic energy, decreased maximum Eady growth rates and decreased poleward heat transport, all suggesting decreased storm track activity. Although *Sobolowski et al.* [2010] obtains a similar, downstream transient eddy response, they find an increase in storm track activity and warming over northern Eurasia during springtime. Reasons for this discrepancy are unclear, but may be due to the year-round snow forcing used by *Sobolowski et al.* [2010]; their restricted fall-season-only integrations show more similarity to our results.

[50] In the second part of the NA response, the decreased transient eddy poleward heat transport results in significant, but short-lived cooling over Siberia and a corresponding increase in upward propagating wave activity, similar to what occurs for EA snowforcing. Thus, transient waves, in addition to stationary waves, are important. A negative AO-like response develops, but remains primarily confined to the stratosphere/upper troposphere. This negative AO-like signal, however, quickly yields to a tropospheric AO-like response of the opposite phase, due to enhancement of the prevailing tropospheric equatorward wave activity and increased wave divergence. This latter result is similar to *Gong et al.* [2003b], who found NA snow anomalies yield a positive AO-like mode at the surface. This response is robust to varying the NA snow forcing and consistent with NCEP/NCAR Reanalysis data, which shows significant positive correlations between November NA snow and the subsequent March AO.

[51] Unlike the NA and EA results, snow forcing experiments for the whole Northern Hemisphere exhibit a weak AO-like response. This is due to a muted wavenumber-1 and -2 response, which is caused by destructive interference between the stationary background wave and the corresponding Rossby wave response. This results in negligible wave activity reaching the stratosphere and much smaller increases in high-latitude geopotential heights, which are unable to propagate down through the troposphere.

[52] Our results add to the growing number of studies that show snow cover is an important land-surface boundary condition, able to affect climate remotely and modulate the dominant mode of NH wintertime atmospheric circulation variability. *Cohen and Barlow* [2005] and *Cohen et al.* [2007] suggest that fall snow cover may have also forced the observed trend in the wintertime (DJF) AO, which exhibited a positive trend for much of the 1970s and 1980s, with historic highs in the early 1990s, and has recently been decreasing. This is consistent with the EA snow-AO relationship, particularly since the early 1990's, as EA SON snow cover has been increasing. Furthermore, the recent decrease in the early springtime (March) AO is consistent with the NA snow-AO relationship, as NA November snow cover has been decreasing (now shown). However, there have been no GCM experiments demonstrating such a relationship. In a companion study, CAM will be used to investigate the relationship between such snow cover and AO trends, using the prescribed snow method presented here, to specify observationally based snow forcing over the latter 20th century. Such entire-year integrations also preserve the multiannual persistence of snow forcing, which may be an important mechanism in the snow-AO relationship, as suggested by observations [*Bojariu and Gimeno*, 2003; R. J. Allen and C. S. Zender, The role of eastern Siberian snow and soil moisture anomalies in multiannual AO/NAO persistence, submitted to *Journal of Geophysical Research*, 2010] and recent model experiments [*Sobolowski et al.*, 2010].

Appendix A: CAM Albedo Parameterization

[53] The surface albedo (α), which is partitioned into direct and diffuse beam for visible (VIS; < 7 μm) and near-infrared

(NIR; $\geq 0.7\ \mu m$) radiation, of each land column is a function of ground cover type, vegetation, soil color and type, soil moisture and snow cover [*Oleson et al.*, 2004]. The albedo effects of snow cover depend on the snow age and the cosine of the solar zenith angle (μ). For new snow with $\mu > 0.5$, the NIR snow albedo (SA) is 0.65; for VIS its 0.95. The direct beam SA is then reduced for $\mu \leq 0.5$ according to

$$\alpha^{\mu}_{snow,\Lambda} = \alpha_{snow,\Lambda} + 0.4 f(\mu)\left[1 - \alpha_{snow,\Lambda}\right], \tag{A1}$$

where Λ is the waveband (NIR or VIS) and $f(\mu)$ is a factor between 0 and 1 (0 for $\mu > 0.5$; $f \rightarrow 1$ as $\mu \rightarrow 0$). Because $[1 - \alpha_{snow,\Lambda}]$ is larger for NIR radiation, the μ dependence on NIR SA will likewise be larger.

[54] Snow cover also affects the albedo of vegetation by reducing the exposed leaf and stem area through ground accumulation and canopy interception. The leaf and stem area indices are adjusted for vertical burying by snow as

$$A = A^{*}\left(1 - f^{snow}_{veg}\right), \tag{A2}$$

where A^* is the leaf/stem area without snow, A is the remaining exposed leaf/stem area and f^{snow}_{veg} is the vertical fraction of vegetation covered by snow (a function of snow depth and the canopy bottom height). These snow-adjusted values are then used to estimate the radiative transfer within the canopy, including fluxes absorbed by the vegetation, reflected by the vegetation, and transmitted through the vegetation.

[55] Three additional optical parameters in the calculation of canopy radiation transfer, including a scattering coefficient (ω) and upscattering parameters for diffuse (β) and direct (β_0) beam radiation, also depend on snow. If $T_{veg} \leq T_f$, where T_{veg} is vegetation temperature and T_f is the freezing temperature of water, then ω, β, and β_0 [see *Oleson et al.*, 2004, equations (3.1) and (3.2)] are weighted combinations of values for vegetation and snow.

[56] To calculate the total ground albedo for direct ($\alpha^{\mu}_{grd,\Lambda}$) and diffuse ($\alpha_{grd,\Lambda}$) radiation, the model uses the snow cover fraction (f_{snow}) to weight the contributions of soil and snow albedos according to

$$\alpha^{\mu}_{grd,\Lambda} = \alpha^{\mu}_{soil,\Lambda}(1 - f_{snow}) + \alpha^{\mu}_{snow,\Lambda} f_{snow} \tag{A3}$$

and

$$\alpha_{grd,\Lambda} = \alpha_{soil,\Lambda}(1 - f_{snow}) + \alpha_{snow,\Lambda} f_{snow}, \tag{A4}$$

where $\alpha^{\mu}_{soil,\Lambda}$ and $\alpha_{soil,\Lambda}$ vary with glacier, lake, wetland and soil surfaces.

[57] **Acknowledgments.** This study was funded by NSF ARC-0714088 and NASA NNX07AR23G, UC Irvine. We thank Chris Fletcher and one anonymous reviewer for their helpful comments that significantly improved this manuscript.

References

Baldwin, M. P., and T. J. Dunkerton (1999), Propagation of the Arctic Oscillation from the stratosphere to the troposphere, *J. Geophys. Res.*, *104*(D24), 30,937–30,946.

Baldwin, M. P., and T. J. Dunkerton (2001), Stratospheric harbingers of anomalous weather regimes, *Science*, *294*, 581–584.

Bojariu, R., and L. Gimeno (2003), The role of snow cover fluctuations in multiannual NAO persistence, *Geophys. Res. Lett.*, *30*(4), 1156, doi:10.1029/2002GL015651.

Cohen, J., and M. Barlow (2005), The NAO, the AO and global warming: How closely related?, *J. Clim.*, *18*, 4498–4513.

Cohen, J., and D. Entekhabi (1999), Eurasian snow cover variability and Northern Hemisphere climate predictability, *Geophys. Res. Lett.*, *26*(3), 345–348.

Cohen, J., A. Frei, and R. D. Rosen (2005), The role of boundary conditions in AMIP-2 simultations of the NAO, *J. Clim.*, *18*, 973–981.

Cohen, J., M. Barlow, P. J. Kushner, and K. Saito (2007), Stratosphere-troposphere coupling and links with Eurasian land surface variability, *J. Clim.*, *20*, 5335–5343.

Collins, W. D., et al. (2004), Description of the NCAR Community Atmosphere Model (CAM 3.0), *Tech. Rep. NCAR/TN-464+STR*, 226 pp., Natl. Cent. for Atmos. Res., Boulder, Colo.

Dewey, K. F. (1977), Daily maximum and minimum temperature forecasts and the influence of snow cover, *Mon. Weather Rev.*, *105*, 1594–1597.

Dickson, R. R., and J. Namias (1976), North American influences on the circulation and climate of the North Atlantic sector, *Mon. Weather Rev.*, *104*, 1255–1265.

Edmon, H. J., Jr., B. J. Hoskins, and M. E. McIntyre (1980), Eliassen-Palm cross sections for the troposphere, *J. Atmos. Sci.*, *37*, 2600–2616.

Feldstein, S. B. (2002), The recent trend and variance increase of the annular mode, *J. Clim.*, *15*, 88–94.

Fletcher, C. G., P. J. Kushner, and J. Cohen (2007), Stratospheric control of the extratropical circulation response to surface forcing, *Geophys. Res. Lett.*, *34*, L21802, doi:10.1029/2007GL031626.

Fletcher, C. G., S. C. Hardiman, P. J. Kushner, and J. Cohen (2009), The dynamical response to snow cover perturbations in a large ensemble of atmospheric GCM integrations, *J. Clim.*, *22*, 1208–1222.

Frei, A., J. A. Miller, and D. A. Robinson (2003), Improved simulations of snow extent in the second phase of the Atmospheric Model Intercomparison Project (AMIP-2), *J. Geophys. Res.*, *108*(D12), 4369, doi:10.1029/2002JD003030.

Fyfe, J. C., G. J. Boer, and G. M. Flato (1999), The Arctic and Antarctic Oscillations and their projected changes under global warming, *Geophys. Res. Lett.*, *26*(11), 1601–1604.

Garfinkel, C. I., and D. L. Hartmann (2010), Tropospheric precursors of anomalous Northern Hemisphere stratospheric polar vortices, *J. Clim.*, *23*, 3282–3299.

Gong, G., D. Entekhabi, and J. Cohen (2002), A large-enemble model study of the wintertime AO-NAO and the role of interannual snow perturbations, *J. Clim.*, *15*, 3488–3499.

Gong, G., D. Entekhabi, and J. Cohen (2003a), Modeled Northern Hemisphere winter climate response to realistic Siberian snow anomalies, *J. Clim.*, *16*, 3917–3931.

Gong, G., D. Entekhabi, and J. Cohen (2003b), Relative impacts of Siberian and North American snow anomalies on the winter Arctic Oscillation, *Geophys. Res. Lett.*, *30*(16), 1848, doi:10.1029/2003GL017749.

Gong, G., D. Entekhabi, J. Cohen, and D. Robinson (2004), Sensitivity of atmospheric response to modeled snow anomaly characteristics, *J. Geophys. Res.*, *109*, D06107, doi:10.1029/2003JD004160.

Hardiman, S. C., P. J. Kushner, and J. Cohen (2008), Investigating the ability of general circulation models to capture the effects of Eurasian snow cover on winter climate, *J. Geophys. Res.*, *113*, D21123, doi:10.1029/2008JD010623.

Haynes, P. H., C. J. Marks, M. E. McIntyre, T. G. Shepherd, and K. P. Shine (1991), On the "downward control" of extratropical diabatic circulations by eddy-induced mean zonal forces, *J. Atmos. Sci.*, *48*, 651–678.

Hoerling, M., J. W. Hurrell, and T. Xu (2001), Tropical origins for recent North Atlantic climate change, *Science*, *292*, 90–92.

Hurrell, J. W., and H. van Loon (1997), Decadal variations in climate associated with the North Atlantic oscillation, *Clim. Change*, *36*, 301–326.

Hurrell, J. W., M. P. Hoerling, A. S. Phillips, and T. Xu (2004), Twentieth century North Atlantic climate change. Part I: Assessing determinism, *Clim. Dyn.*, *23*, 371–389.

Klingaman, N. P., B. Hanson, and D. J. Leathers (2008), A teleconnection between forced Great Plains snow cover and European winter climate, *J. Clim.*, *21*, 2466–2483.

Kushnir, Y., W. A. Robinson, P. Chang, and A. W. Robertson (2006), The physical basis for predicting Atlantic sector seasonal-to-interannual climate variability, *J. Clim.*, *19*, 5949–5970.

Leathers, D. J., and D. A. Robinson (1993), The association between extremes in North American snow cover extent and United States temperature, *J. Clim.*, *6*, 1345–1355.

Leathers, D. J., A. W. Ellis, and D. A. Robinson (1995), Characteristics of temperature depressions associated with snow cover across the northeast United States, *J. Appl. Meteorol.*, *34*, 381–390.

Limpasuvan, V., D. W. J. Thompson, and D. L. Hartmann (2004), The life cycle of the Northern Hemisphere sudden stratospheric warmings, *J. Clim.*, *17*, 2584–2596.

Lindzen, R. S., and B. Farrell (1980), A simple approximate result for the maximum growth rate of baroclinic instabilities, *J. Atmos. Sci.*, *37*, 1648–1654.

McFadden, J. D., and R. A. Ragotzkie (1967), Climatological significance of albedo in central Canada, *J. Geophys. Res.*, *72*(4), 1135–1143.

McFarlane, N. A. (1987), The effect of orographically excited wave drag on the general circulation of the lower stratosphere and troposphere, *J. Atmos. Sci.*, *44*, 1775–1800.

Miller, R. L., G. A. Schmidt, and D. T. Shindell (2006), Forced annular variations in the 20th century Intergovernmental Panel on Climate Change Fourth Assessment Report models, *J. Geophys. Res.*, *111*, D18101, doi:10.1029/2005JD006323.

Oleson, K. W., et al. (2004), Technical description of the Community Land Model (CLM), *Tech. Rep. NCAR/TN-461+STR*, 174 pp., Natl. Cent. for Atmos. Res., Boulder, Colo.

Osborn, T. J. (2004), Simulating the winter North Atlantic Oscillation: The roles of internal variability and greenhouse gas forcing, *Clim. Dyn.*, *22*, 605–623.

Plumb, R. A. (1985), On the three-dimensional propagation of stationary waves, *J. Atmos. Sci.*, *42*, 217–229.

Polvani, L. M., and D. W. Waugh (2004), Upward wave activity flux as a precursor to extreme stratospheric events and subsequent anomalous surface weather regimes, *J. Clim.*, *17*, 3548–3554.

Rind, D., J. Perlwitz, P. Lonergan, and J. Lerner (2005a), AO/NAO response to climate change: 2. Relative importance of low- and high-latitude temperature change, *J. Geophys. Res.*, *110*, D12108, doi:10.1029/2004JD005686.

Rind, D., J. Perlwitz, and P. Lonergan (2005b), AO/NAO response to climate change: 1. Respective influences of stratospheric and tropospheric climate changes, *J. Geophys. Res.*, *110*, D12107, doi:10.1029/2004JD005103.

Ringler, T. D., and K. H. Cook (1999), Understanding the seasonality of orographically forced waves: Interaction between mechanical and thermal forcing, *J. Atmos. Sci.*, *56*, 1154–1174.

Robertson, A. W. (2001), Influence of ocean-atmosphere interaction on the Arctic Oscillation in two general circulation models, *J. Clim.*, *14*, 3240–3254.

Robertson, A. W., C. R. Mechoso, and Y.-J. Kim (2000), The influence of Atlantic sea surface temperature anomalies on the North Atlantic Oscillation, *J. Clim.*, *13*, 122–138.

Rodwell, M. J., D. P. Rowell, and C. K. Folland (1999), Oceanic forcing of the wintertime North Atlantic Oscillation and European climate, *Nature*, *398*, 320–323.

Roesch, A. (2006), Evaluation of surface albedo and snow cover in AR4 coupled climate models, *J. Geophys. Res.*, *111*, D15111, doi:10.1029/2005JD006473.

Saito, K., and J. Cohen (2003), The potential role of snow cover in forcing interannual variability of the major Northern Hemisphere mode, *Geophys. Res. Lett.*, *30*(6), 1302, doi:10.1029/2002GL016341.

Saito, K., J. Cohen, and D. Entekhabi (2001), Evolution of atmospheric response to early-season Eurasian snow cover anomalies, *Mon. Weather Rev.*, *129*, 2746–2760.

Selten, F. M., G. W. Branstator, H. A. Dijkstra, and M. Kliphuis (2004), Tropical origins for recent and future Northern Hemisphere climate change, *Geophys. Res. Lett.*, *31*, L21205, doi:10.1029/2004GL020739.

Shaw, T. A., M. Sigmond, T. G. Shepherd, and J. F. Scinocca (2009), Sensitivity of simulated climate to conservation of momentum in gravity wave drag parameterization, *J. Clim.*, *22*, 2726–2742.

Shindell, D. T., R. L. Miller, G. A. Schmidt, and L. Pandolfo (1999), Simulation of recent northern winter climate trends by greenhouse-gas forcing, *Nature*, *399*, 452–455.

Sigmond, M., J. F. Scinocca, and P. J. Kushner (2008), Impact of the stratosphere on tropospheric climate change, *Geophys. Res. Lett.*, *35*, L12706, doi:10.1029/2008GL033573.

Smith, K. L., C. G. Fletcher, and P. J. Kushner (2010), The role of linear interference in the Annular Mode response to extratropical surface forcing, *J. Clim.*, doi:10.1175/2010JCLI3606.1, in press.

Sobolowski, S., G. Gong, and M. Ting (2007), Northern Hemisphere winter climate variability: Response to North American snow cover anomalies and orography, *Geophys. Res. Lett.*, *34*, L16825, doi:10.1029/2007GL030573.

Sobolowski, S., G. Gong, and M. Ting (2010), Modeled climate state and dynamic responses to anomalous North American snow cover, *J. Clim.*, *23*, 785–799.

Stenchikov, G., A. Robock, V. Ramaswamy, M. D. Schwarzkopf, K. Hamilton, and S. Ramachandran (2002), Arctic Oscillation response to the 1991 Mount Pinatubo eruption: Effects of volcanic aerosols and ozone depletion, *J. Geophys. Res.*, *107*(D24), 4803, doi:10.1029/2002JD002090.

Stenchikov, G., K. Hamilton, R. J. Stouffer, A. Robock, V. Ramaswamy, B. Santer, and H.-F. Graf (2006), Arctic Oscillation response to volcanic eruptions in the IPCC AR4 climate models, *J. Geophys. Res.*, *111*, D07107, doi:10.1029/2005JD006286.

Thompson, D. W. J., and J. M. Wallace (1998), The Arctic Oscillation signature in the wintertime geopotential height and temperature fields, *Geophys. Res. Lett.*, *25*(9), 1297–1300.

Thompson, D. W. J., and J. M. Wallace (2000), Annular modes in the extratropical circulation. Part I: Month to month variability, *J. Clim.*, *13*, 1000–1016.

Thompson, D. W. J., and J. M. Wallace (2001), Regional climate impacts of the Northern Hemisphere annular mode, *Science*, *293*, 85–89.

Thompson, D. W. J., J. M. Wallace, and G. C. Hegerl (2000), Annular modes in the extratropical circulation. Part II: Trends, *J. Clim.*, *13*, 1018–1036.

Trenberth, K. E. (1991), Storm tracks in the Southern Hemisphere, *J. Atmos. Sci.*, *48*, 2159–2178.

Wagner, A. J. (1973), The influence of average snow depth on monthly mean temperature anomaly, *Mon. Weather Rev.*, *101*, 624–626.

Wallace, J. M., and D. S. Gutzler (1981), Teleconnections in the geopotential height field during the Northern Hemisphere winter, *Mon. Weather Rev.*, *109*, 784–812.

Walland, D. J., and I. Simmonds (1996), Sub-grid scale topography and the simulation of Northern Hemisphere snow cover, *Int. J. Climatol.*, *16*, 961–982.

R. J. Allen and C. S. Zender, Department of Earth System Science, University of California, Irvine, CA 92697, USA. (rjallen@uci.edu)